ChemComm

CrossMark
◀ click for updates

The surface chemistry of metal–organic frameworks

Christina V. McGuire and Ross S. Forgan*

Metal–organic frameworks (MOFs) have received particular attention over the last 20 years as a result of their attractive properties offering potential applications in a number of areas. Typically, these characteristics are tuned by functionalisation of the bulk of the MOF material itself. This *Feature Article* focuses instead on modification of MOF particles at their surfaces only, which can also offer control over the bulk properties of the material. The differing surface modification techniques available to the synthetic chemist will be discussed, with a focus on the effect of surface modification of MOFs on their fundamental properties and application in adsorption, catalysis, drug delivery and other areas.

1. Introduction

Metal–organic frameworks (MOFs) comprise metal ions or metal clusters linked by organic ligands, or struts, into network structures which often exhibit permanent porosity.[1] The ability of MOFs to capture and store molecular species has led to their application in CO_2 sequestration,[2] storage of hydrogen[3] and other gases,[4] separations science,[5] drug delivery,[6] heterogeneous catalysis[7] and electronic devices.[8] Efforts to modify and enhance their properties have focused mostly on introducing functionality to the inner pore

School of Chemistry, Joseph Black Building, University of Glasgow, University Avenue, Glasgow, G12 8QQ, UK. E-mail: ross.forgan@glasgow.ac.uk; Web: www.forganlab.com, Twitter: @forganross

surfaces, *i.e.*, throughout the bulk material. Examples include the use (Fig. 1a) of cyclodextrins as ligands, which result in MOFs with huge numbers of nucleophilic hydroxyl units to effect transient chemisorption of CO_2,[9] the incorporation (Fig. 1b) of urea moieties into struts to give MOFs which act as H-bond donor organocatalysts,[10] and the separation (Fig. 1c) of volatile hydrocarbons over an iron dioxidoterephthalate MOF through varying levels of interaction with coordinatively unsaturated iron centres.[11] Whilst this approach has successfully generated many functional MOFs, there have been considerably fewer examples of synthetic chemists addressing the outer surfaces of MOF crystals with a view to imparting new bulk properties.[12]

It is perhaps surprising that the surface chemistry of MOFs remains relatively unexplored, given the wealth of advanced

Christina McGuire joined the Forgan Group in 2013, during the final year of her undergraduate degree at the University of Glasgow, where she carried out research into the surface chemistry and crystal growth control of MOFs. After receiving her BSc (Hons) degree in 2014, she has taken up a research position at the Łódź University of Technology, Poland.

Christina V. McGuire

Ross Forgan is a Royal Society University Research Fellow in the School of Chemistry at the University of Glasgow. After receiving MChem (Hons) and PhD degrees from the University of Edinburgh in 2004 and 2008, under the supervision of Prof. Peter Tasker, he spent three years as a postdoctoral researcher in the group of Prof. Sir J. Fraser Stoddart at Northwestern University, USA. In 2011 he returned to Scotland as a postdoctoral researcher in the

Ross S. Forgan

group of Prof. Lee Cronin at the University of Glasgow, and took up his current independent position in 2012. His research group is interested in the crystallisation and surface chemistry of MOFs, as well as their materials properties and biomimetic applications.
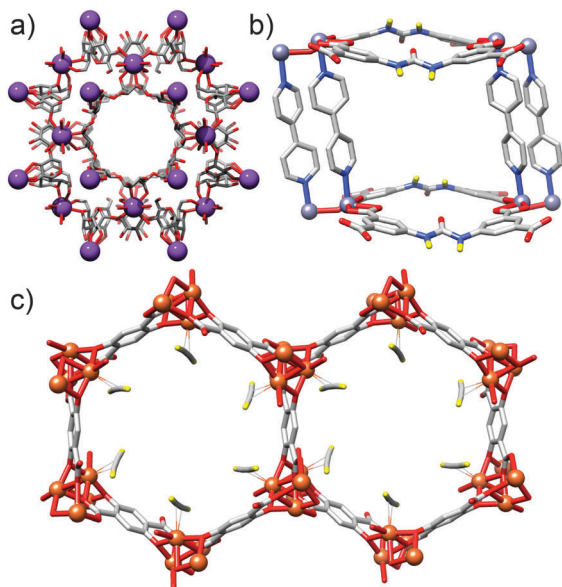
Fig. 1 Sections of the solid-state structures of (a) CD-MOF-2, whose surfeit of pendant hydroxyl units facilitates transient chemisorption of CO_2, (b) NU-601, a urea functionalised MOF which acts as a heterogeneous organocatalyst, and (c) iron dioxidoterephthalate, binding acetylene through interactions with coordinatively unsaturated Fe^{2+} cations. Redrawn from CSD depositions LAJLEP, HAPHUD and SARGID, in turn.

functional materials resulting from alternative nanomaterials with appropriate surface decoration. For example, mechanised silica nanoparticles utilised in drug delivery can have exquisite surface ligands to effect targeted, stimuli-responsive release,[13] whilst the incorporation of biomolecules onto noble metal nanoparticles significantly enhances both their self-assembly and sensory properties.[14]

This *Feature Article* examines attempts to chemically address and modify the surfaces of MOF materials with a view to altering their bulk properties. The varying synthetic and self-assembly approaches will be considered in three groupings: (i) surface modification during MOF synthesis through coordination modulation, (ii) post-synthetic surface modification, and (iii) MOFs grown directly on the surfaces of others in the form of epitaxial and surface growth.

2. Surface modification by coordination modulation

The surfaces of MOF particles can be addressed during their synthesis using a technique called coordination modulation. The method of coordination modulation (Fig. 2) simply involves the introduction of a monodentate ligand, which possesses similar chemical functionality to the existing multidentate organic ligands, into the MOF synthesis reaction mixture.

Modulation of the coordination equilibrium arises from the introduced ligand, known as a modulator, competing with the MOF's bridging ligands for coordination to the metal ions, and so a modulator can act either to promote crystal growth or to inhibit it. In the case of the former, the modulator controls
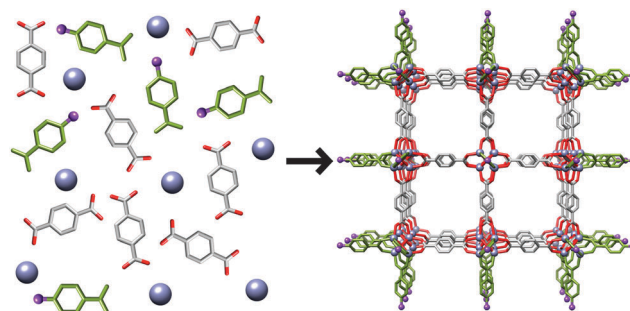

Fig. 2 Schematic illustration of coordination modulation, where a monodentate ligand, or modulator, caps MOF crystal growth, using MOF-5 as an idealised example.

nucleation to achieve MOF crystals of varying sizes depending on concentration. In the latter case, the modulator can be thought of as a capping agent, which terminates the network structure by coordinating to the metal site where a polydentate ligand would normally be found. The capping agent's lack of further binding sites prevents further assembly of the network and so control over the MOF crystal size *and* surface chemistry is achieved. The functionality of a capping modulator is therefore confined to the surface, with the potential to alter the bulk properties of the modulated MOF particles, so coordination modulation is a powerful tool for addressing the surfaces of MOF crystals during synthesis.

2.1 Coordination modulation

Fischer and co-workers have examined[15] the use of a monocarboxylic acid as a surface capping agent for the prototypical material MOF-5, $[Zn_4O(1,4\text{-}bdc)_3]_n$ (bdc = benzenedicarboxylate). MOF-5 is a cubic framework with octahedral secondary building units (SBUs) comprised of Zn_4O tetrahedra; each cluster is linked by 1,4-bdc ligands, and it was hypothesised that the modulator, *p*-perfluoromethylbenzenecarboxylate (pfmbc), would bind to open Zn positions, inhibit crystal growth and so be installed on the surface of the MOF (see Fig. 2 for a schematic illustration). In a solvothermal synthesis in *N,N'*-diethylformamide, crystals of MOF-5 obtained from a control solution grew to sizes in excess of 350 nm, while crystals obtained from a modulated synthesis were less than half the size of the control crystals. A 2 : 1 ratio of pfmbc to 1,4-bdc produced crystals with an average size of 100 nm, whilst increasing this ratio to 5 : 1 resulted in crystals with an average size of 150 nm. This initial study confirmed the effective use of capping agents to stabilise the growth of MOF crystals and the importance of competing ligands at the coordination site in influencing the size of MOF particles. The positioning of the modulator solely at the crystal surface, however, was not directly confirmed. The perfluorinated modulator would be expected to generate a strongly hydrophobic MOF crystal if, as expected, it was deposited on the surface as a capping agent.

The simplicity of the coordination modulation approach has led to its application in a number of other MOF systems, a cross-section of which is described below. Kitagawa *et al.* examined[16]

the modulated synthesis of HKUST-1, $[Cu_3(1,3,5-btc)_2]_n$, where btc = benzenetricarboxylate, under microwave irradiation in butanol. Using copper acetate as the metal source resulted in a poorly crystalline, gel-like material in the absence of a modulator, but addition of n-dodecanoic acid yielded well defined cubic crystals, whose size increased (20 nm up to 1 μm) as the ratio of modulator to ligand increased. The modulator may act as a capping agent but also compete with the ligand for access to the metal cations, slowing nucleation and crystallisation. When copper nitrate is used[17] as the metal source, the rate of nucleation is much slower, and so addition of n-dodecanoic acid influences the morphology of the HKUST-1 crystals rather than size (1–5 μm). As the concentration of modulator increases, the crystal morphology changes from octahedron, to cuboctahedron, to cube. A coarse-grain modelling methodology was used to conclude that the modulator regulated the relative energies of two types of nearest neighbour sites in such a way that they became the favoured nucleation sites. Increasing the tendency for nucleation to occur at these sites led to a morphology transition from octahedron to cube associated with the concentration of n-dodecanoic acid during synthesis. The change in crystal morphology has the effect of exposing certain crystal facets, potentially allowing for control over surface reactivity.

Liu and Guo studied[18] the formation of HKUST-1 under hydrothermal (water–ethanol solvent) conditions, and found that addition of even one equivalent of sodium formate with respect to 1,3,5-btc lowered crystal size from 20 μm to 300 nm. Crystal size could be further lowered with up to 3 equivalents of sodium formate; addition of larger quantities resulted in new phases forming. Remarkably similar results were reported[19] by Zhang et al. in the synthesis of frameworks of the type $[Ln(1,3,5-btc)(H_2O)]_n$, Ln = Dy^{3+}, Eu^{3+}, Tb^{3+} or mixtures of the three, synthesised in aqueous N,N'-dimethylformamide (DMF) with sodium formate and acetate as modulators. Both groups concluded that the use of basic carboxylate salts, rather than the parent acids, increased the pH of the reaction mixtures, facilitating deprotonation of the 1,3,5-btc ligands and thus the rapid nucleation of smaller crystals. However, pH alteration of reaction mixtures with bases that could not act as capping ligands, for example triethylamine, did not result in MOF particles as small as those of sodium formate or acetate. Clearly a synergistic effect is in play; a basic modulator can both speed up nucleation and then cap the crystal at the surface (Fig. 3).

This theory was successfully tested in the synthesis of nanoscale particles of MOF-5 and HKUST-1, while Gascon et al. used[20] in situ X-ray scattering techniques alongside DFT calculations to elucidate the mechanism of diethylamine modulation of the zeolitic imidazolate framework ZIF-7 – $[Zn(bim)_2]_n$ where bim = benzimidazolate – again finding increased base concentration enhanced crystallisation kinetics.

In addition, coordination modulation has been applied to a range of metal carboxylate MOFs (Fig. 4). Sodium acetate can be used[21] to modulate the synthesis of MIL-68(In), $[In(OH)(1,4-bdc)]_n$, decreasing both the length and diameter of the hexagonal nanorods formed during solvothermal synthesis. Burrows et al. showed[22] that hydrothermal synthesis of MIL-101(Cr), $[Cr_3O(OH)(H_2O)_2(1,4-bdc)_3]_n$,
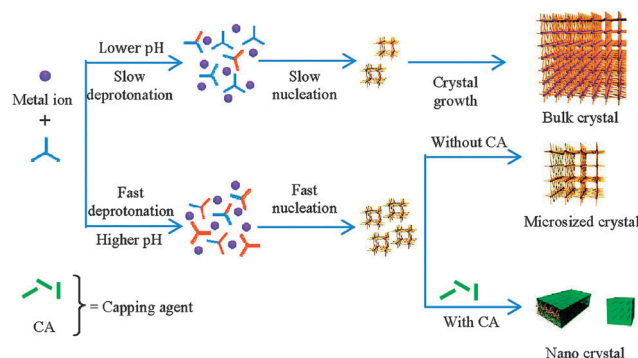

Fig. 3 Schematic model proposed by Zhang et al. to explain the dual effects of pH control and crystal capping during coordination modulation. Reprinted with permission from ref. 19b. Copyright (2012) American Chemical Society.

can be modulated by a variety of monocarboxylic acids, producing nanoparticles of size 19–84 nm. When the modulator is the only synthetic parameter varied, nanoparticle size correlates well with the pK_a of the modulator – the lower the pK_a, the more deprotonated the modulator – which can compete more strongly with the 1,4-bdc ligands for the Cr cations, slowing nucleation and increasing crystal size. Acetic acid has been used[23] as a modulator in the solvothermal synthesis of NH$_2$-MIL-53(Al), $[Al(OH)(2-NH_2-1,4-bdc)]_n$, facilitating the formation of needles aligned in the [001] direction, suggesting selective capping of certain crystal faces.

Zirconium carboxylates, in particular the UiO series of the general formula $[Zr_6O_4(OH)_4(L)_6]_n$, where L is a linear dicarboxylate ligand, can be modulated from the nanoscale all the way up to crystals suitable for single crystal X-ray diffraction. Behrens et al. described[24] the use of benzoic acid and acetic acid to produce a range of MOFs of varying sizes, from nano- to microscale, with improved crystallinity compared to unmodulated systems. Utilising 30 equivalents of benzoic acid as modulator in a solvothermal synthesis resulted in 100 μm crystals of UiO-68-NH$_2$, where the ligand is 2'-amino-1,1':4',1''-terphenyl-4,4''-dicarboxylate, which proved suitable for X-ray diffraction analysis. Modulation is now commonplace in the synthesis of Zr carboxylate MOFs, and Behrens et al. suggest that excess modulator can be found on the outer surfaces of the Zr MOF crystals.

Zeolitic imidazolate frameworks (ZIFs) can also be prepared by modulated synthesis. Wiebcke et al. demonstrated[25] that variously sized particles of ZIF-8, $[Zn(mim)_2]_n$ where mim = 2-methylimidazolate, can be prepared in a room temperature synthesis in methanol with the following modulators: n-butylamine (10–65 nm particles), sodium formate (1–2 μm particles), and 1-methylimidazole (1 μm particles). This example demonstrates that modulation can occur in MOFs with ligands that are not carboxylate functionalised, and also that modulators with different donor units to the linker ligand can be utilised. Light scattering was used to monitor the n-butylamine modulated self-assembly process in situ, and it was found that, in the early stages of growth, a narrowing of particle size distribution occurs, implying initial effective surface capping of the MOF crystallites
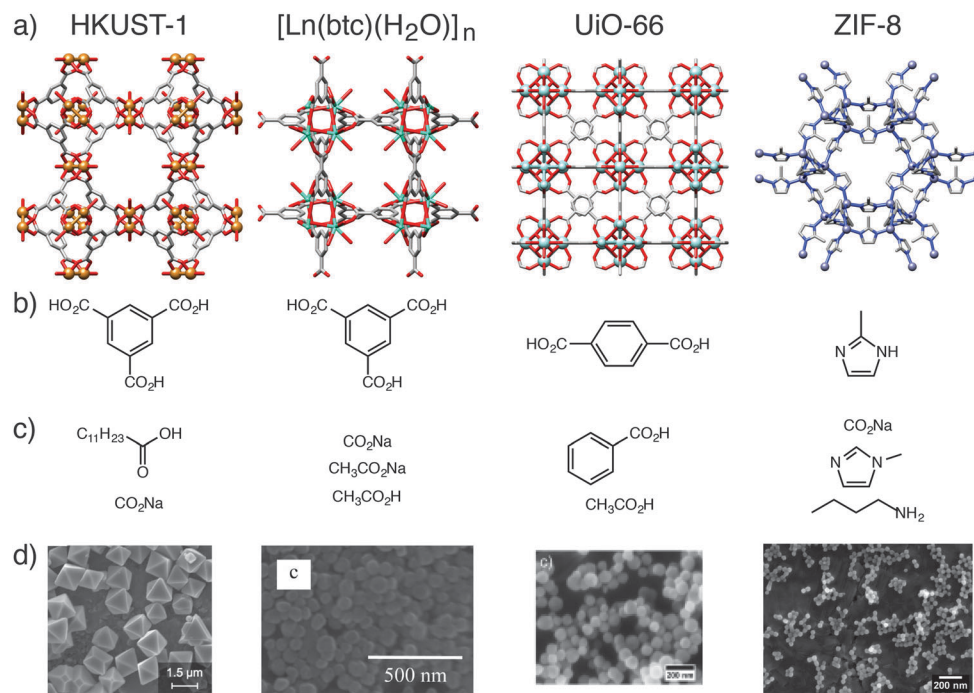
Fig. 4 Examples of MOFs which have been synthesised using the coordination modulation method. (a) Labelled packing diagrams of their crystal structures. (b) Chemical structures of the MOF ligand and (c) the modulators employed for each example. (d) Electron microscope images of the resulting micro and nanoparticles of the MOFs. Scale bars are 1.5 μm (HKUST-1), 500 nm [Dy(1,3,5-btc)(H$_2$O)]$_n$, 200 nm (UiO-66) and 200 nm (ZIF-8). Crystal structures redrawn from CCDC depositions FIQCEN (HKUST-1), YEMIAC [Dy(1,3,5-btc)(H$_2$O)]$_n$, RUBTAK (UiO-66) and VELVOY (ZIF-8). Microscopy images in part (d) HKUST-1: reprinted (adapted) with permission from ref. 17. Copyright (2011) American Chemical Society. [Dy(1,3,5-btc)(H$_2$O)]$_n$: reprinted (adapted) with permission from ref. 19b. Copyright (2012) American Chemical Society. UiO-66: reprinted (adapted) with permission from ref. 24. Copyright (2011) John Wiley and Sons. ZIF-8: reprinted (adapted) with permission from ref. 25. Copyright (2011) American Chemical Society.

by the modulator. In contrast, the same group examined[26] the formate modulated synthesis of ZIF-8 in methanol under solvothermal conditions, where the formate modulator was found to act as a base, rather than a surface capping agent, in the assembly of crystals up to 100 μm in diameter.

It should be noted that the approach of adding monovalent ligands into MOF syntheses does not always result in selective surface capping. Zhou *et al.* demonstrated[27] that incorporation of ligand fragments into the synthesis of NOTT-101 (copper cations linked by 1,1′:4′,1″-terphenyl-3,3″,5,5″-tetracarboxylate units, see Fig. 5a) resulted in defect formation throughout the bulk of the MOF, rather than surface termination. The incorporation of monomeric isophthalate fragments throughout the framework in place of linker units (Fig. 5b) increases the overall pore volume of the MOF and generates mesopores, while also providing a route towards pore functionalisation through a variety of functional groups attached to the isophthalate.

Such defects induced by missing linkers are also known to pervade through Zr carboxylate MOFs, and can be deliberately induced in UiO-66, a cubic framework of formula [Zr$_6$O$_4$(OH)$_4$-(1,4-bdc)$_6$]$_n$, by addition of trifluoroacetic acid (TFA) to its synthesis. De Vos and co-workers showed[28] that while other monovalent acids act as crystal growth modulators to produce more crystalline MOFs, TFA could induce defects by replacing 1,4-bdc ligands at the Zr clusters. Activation at 320 °C removes the TFA defects, leaving an enhanced Lewis acidic catalytic
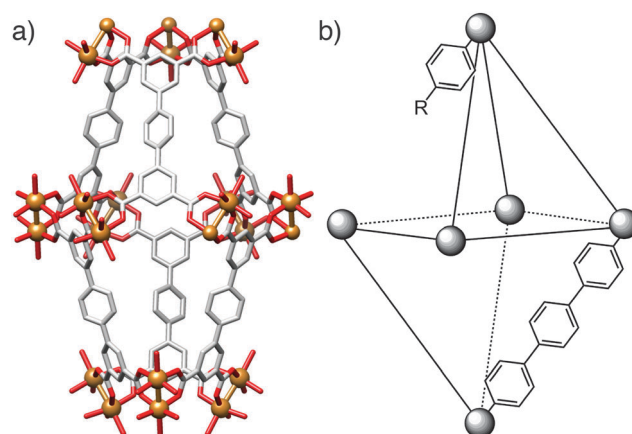

Fig. 5 (a) Section of the crystal structure of NOTT-101 (redrawn from CCDC deposition CESFOW). (b) Simplified diagram to illustrate the introduction of defects within NOTT-101 when isophthalate modulators are incorporated into the synthesis of the MOF, generating mesopores with additional functional groups (labelled R).

material compared to untreated UiO-66, with as many as 2 vacancies per Zr cluster. Improved conversions in the cyclisation of citronellol and the Meerwein reduction of 4-*tert*-butylcyclohexanone with isopropanol were attributed to the increased availability of catalytic sites in the modulated material. TFA was found to be the most effective agent to

induce defects when compared to other similar acids, with its very low pK_a postulated as the reason for its efficacy.

Clearly the coordination modulation protocol can have differing outcomes in different systems, with surface capping, increased crystal growth and defect inducement all possible, and so careful choice of modulator is required, taking into account not only the coordinative nature of the modulator, but also its effect on the pH of the synthetic mixture and the rate of crystallisation. Ostwald ripening of kinetically produced, modulated nanoparticles may explain the formation larger crystals with well-defined morphologies and sizes. This effect was postulated by Guo and Liu to be the driving force[29] for the assembly of flower-like crystals of $[Ln(1,3,5\text{-btc})(H_2O)]_n$ coordination polymers (Ln = Dy^{3+} or Tb^{3+} in this case) in a synthesis modulated by sodium acetate, where rapidly formed nanoparticles accumulated into two dimensional nanosheets with their own surface-attached nanoparticles. It may also be the case that many modulated syntheses do not result in surface attachment of the modulator, and so further studies in this area are essential.

2.2 Face selective coordination modulation

When a MOF has multiple types of ligand and hence multiple types of surface, for example, pillared MOFs comprised of metal cations, acid linkers and nitrogen-donor pillars, choosing a modulator which shares its functionality with one type of ligand is a way to attain anisotropic crystal growth. The tetragonal MOF, $[Cu_2(1,4\text{-ndc})_2(\text{dabco})]_n$ (ndc = naphthalenedicarboxylate, dabco = 1,4-diazabicyclo[2.2.2]octane) consists of dimeric copper paddlewheel SBUs linked by 1,4-ndc ligands to form a two dimensional grid, while axial dabco ligands connect these grids via coordination to copper cations to develop the 3D structure. The four [100] crystal surfaces are capped with 1,4-ndc ligands whilst the other two [001] surfaces have terminal dabco ligands. Crystal growth in the [001] and [100] directions arises from dabco–Cu interactions and 1,4-ndc–Cu interactions respectively.

Kitagawa et al. demonstrated[30] that crystal growth of $[Cu_2(1,4\text{-ndc})_2(\text{dabco})]_n$ could be suppressed in the [100] direction as a result of competitive interactions between the modulator added to the solvothermal synthesis, acetic acid, and 1,4-ndc molecules at Cu sites. Both 1,4-ndc and acetic acid possess carboxylate groups, giving rise to competitive interactions and selective surface capping. Conversely, the dabco–Cu coordination sites were unaffected by the modulator and so the resultant crystals had rod-like morphology, with the nanorods oriented in the [001] direction and, presumably, terminal acetate ligands on the [100] surfaces. Similar results were found[31] with the analogous $[Zn_2(1,4\text{-ndc})_2(\text{dabco})]_n$ material, with nanorods formed under microwave heating with n-dodecanoic acid as modulator.

This concept was extended by Do et al., who also investigated[32] the modulation of $[Cu_2(1,4\text{-ndc})_2(\text{dabco})]_n$ with acetic acid, to address the [100] crystal surfaces, and pyridine, to address the [001] faces (Fig. 6). Addition of equimolar amounts of acetic acid and pyridine to the solvothermal synthesis resulted in uniform modulation and the formation of nanocubes. Nanorods resulted when acetic acid was the sole modulator, as per Kitagawa's previous results, and pyridine modulated samples generated nanosheets,
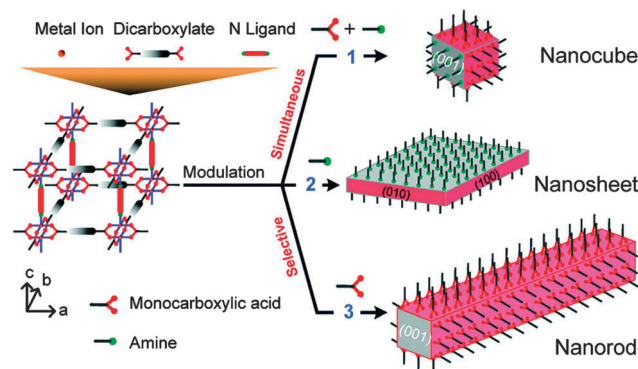

Fig. 6 The effect on crystal shape of varying the ratios of face-selective carboxylic acid and amine modulators during the synthesis of pillared MOFs. Reprinted with permission from ref. 32. Copyright (2012) American Chemical Society.

as a result of capping the [001] faces and only allowing crystal growth along the [100] faces. Selective installation of modulators on different faces of MOFs could potentially regulate adsorptive and catalytic properties associated with individual pore openings and channels.

2.3 Applications of modulated MOFs

Any effects of coordination modulation on the properties of MOFs have largely been as a result of the change in particle size, rather than specific surface chemistry, although the ability to produce surface-capped, monodisperse particles rather than intergrown crystals tends to enhance gas uptake, as described for nanosized MIL-101(Cr)[22] and HKUST-1.[16] Kitagawa et al. have recently reported[33] a remarkable and unexpected property of modulated MOF particles – the so-called shape-memory effect, typically associated with polymers and metal alloys – where nanoscale, or "downsized" MOF crystals are able to retain their shape after adapting to house guest molecules. In flexible porous systems, uptake of guest molecules causes the framework to adopt an "open-phase" configuration in order for the guests to fit within the pores. Upon removal of these guest molecules, the framework's pores would normally be expected to revert back to the original, more stable "closed-phase". Contrary to this usual operating cycle, in the examined modulated crystals the open phase was retained after desorption of the guest molecules and was isolable, with the closed phase regenerated after heating, completing the shape-memory cycle (Fig. 7).

Two different frameworks, $[Cu_2(1,4\text{-bdc})_2(4,4'\text{-bipy})]_n$ (bipy = bipyridine) and $[Cu_2(1,4\text{-bdc})_2(1,2\text{-bpe})]_n$ (bpe = bis(4-pyridyl)-ethylene) were synthesised in the presence of acetic acid, yielding nano- and mesosized crystals (the authors define the meso prefix as denoting dimensions between 100 nm and 1 μm). Several samples were produced, all in the open configuration, by varying the concentration of acetic acid used, with crystal sizes ranging from 50 nm to 300 nm for the 4,4'-bipy-based framework and 50 nm to 700 nm for the 1,2-bpe-based system. The crystals formed in the absence of acetic acid were on the order of micrometres. Following guest molecule desorption and drying,
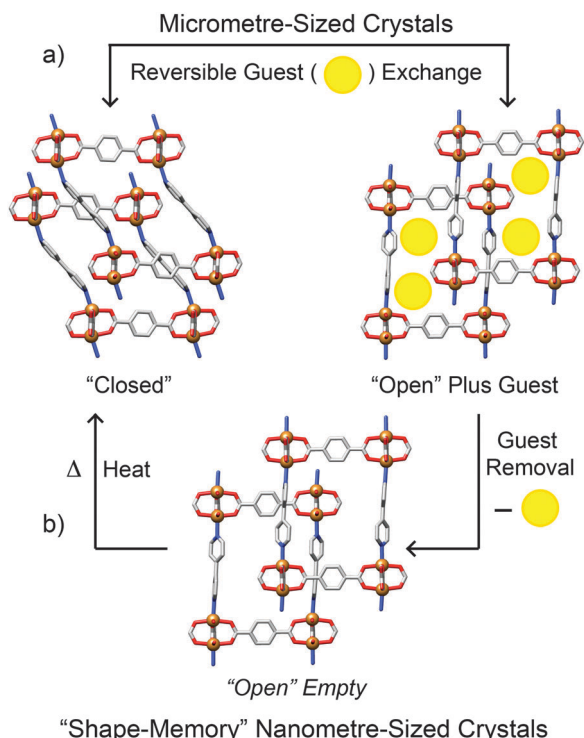
Micrometre-Sized Crystals

a) Reversible Guest (⬤) Exchange

"Closed"   "Open" Plus Guest

Δ | Heat   Guest Removal −

b)

"Open" Empty

"Shape-Memory" Nanometre-Sized Crystals

Fig. 7 Guest sorption/desorption behavior of the flexible MOF [Cu$_2$(1,4-bdc)$_2$(4,4′-bipy)]$_n$. (a) Micrometre sized crystals show reversible guest exchange from its guest-free, closed form to its guest bound, open form. (b) Nanometre sized crystals exhibit a shape memory effect upon removal of guests, retaining the open phase in absence of guests before returning to the closed phase after thermal treatment. The closed phase is drawn from CCDC deposition NEJSIG and the open phase from CCDC deposition NEJSAY (methanol solvated).

the bulk microcrystals and the largest (300 nm) mesocrystals of the 4,4′-bipy framework adopted the expected closed configurations. Open and closed phases were observed for the crystals of intermediary size, while the open configuration was retained completely in the smaller meso- and nanocrystals which only reverted to the closed phase after being heated to 200 °C.

The 1,2-bpe framework behaved a little differently. Firstly, the largest (700 nm) crystal did retain its open configuration despite being over twice the size of the largest 4,4′-bipy crystal. Secondly, the downsized 1,2-bpe crystals did not adopt the closed configuration when heated to 200 °C. This structural rigidity illustrates the effect of crystal downsizing in inhibiting the flexibility of the framework. In the bulk microcrystal, the activation energy of the transition from open- to closed-phase is low enough for the transition to occur spontaneously, so the closed configuration is adopted immediately on guest molecule desorption. Modulation of the crystals increases this activation energy and thermal treatment is required to overcome this energy barrier, explaining the stability of the empty open phase observed.

The ability to control MOF particle size and surface chemistry makes coordination modulation a powerful protocol, with unexpected enhancements of properties as crystal sizes are decreased. Further studies could also lead to the development of synthetic methods towards MOFs with certain surface

components, crystal facets and morphologies. The technique may also endow greater control of particle self-assembly, as MOF surfaces become targets for further functionalisation. Granick *et al.* have already demonstrated interesting assembly properties of modulated ZIF-8 particles, forming[34] hexagonally packed superlattices of crystals with narrow size distributions and inducing[35] chain-like structures under electric fields. With a greater control of surface chemistry, even more complex self-assembled structures could result, but further fundamental studies will be required to confirm the surface attachment of modulators, as this is not guaranteed in each case.

3. Post-synthetic surface modification

Carrying out chemical transformations on previously synthesised MOFs – known as post-synthetic modification (PSM) – has already proven a robust and versatile methodology for introducing functionality into MOFs.[36] Whilst the majority of examples reported to date relate to bulk functionalisation, a number of differing approaches have been conceived to limit post-synthetic modification to the surfaces of MOF particles only, which still impart desirable bulk properties to the resulting surface-modified MOFs.

3.1 Surface modification with polymers and silica

Many of the initial MOF surface post-synthetic modification reports focus on stabilising MOF nanoparticles (NPs) for use in medical treatments and imaging.[37] In one of the earliest studies, Lin and co-workers made use of steric effects to post-synthetically modify MOF nanoparticles of the general formula [Ln(1,4-bdc)$_{1.5}$(H$_2$O)$_2$]$_n$, where Ln = Eu^{3+}, Gd^{3+}, or Tb^{3+} ions, which were utilised as imaging and molecule delivery agents.[38] The surfaces of these MOF NPs were functionalised (Fig. 8a and b) by treating them with poly(vinylpyrrolidone) (PVP), a long polymer chain which added only to the surface of the framework owing to the size of the polymer relative to the MOF's pores. Although this initial step was a surface PSM process in itself, it was used to prepare the Ln MOFs for a subsequent coating of silica, by the established method of basic hydrolysis of tetraethylorthosilicate (TEOS). The silica acts not only to protect the MOF against decomposition, but also as a medium for the anchoring of further surface functionality – in this case, monomeric Tb complexes were attached for imaging purposes and sensing of dipicolinic acid (DPA). Slow dissolution of the hybrids allowed release of Ln cations into cells.

This PVP/silica approach was also successfully applied to nanoparticulate [Mn(1,4-bdc)(H$_2$O)$_2$]$_n$, where the Mn^{2+} centres of the MOF act as MRI contrast agents.[39] Both fluorescent Rhodamine B moieties and targeting c(RGDfK) peptides were grafted (Fig. 8c and d) to the silica-coated surface, which induces selective uptake into human colon cancer cells (HT-29 cell line) and facilitates enhanced imaging. Similarly, nanoparticles of a dicarboxylic acid cisplatin prodrug linked by Tb^{3+} ions were silica coated, with c(RGDfK) peptides targeting agents subsequently attached to yield materials which were selectively taken up by the same HT-29 cell line.[40]
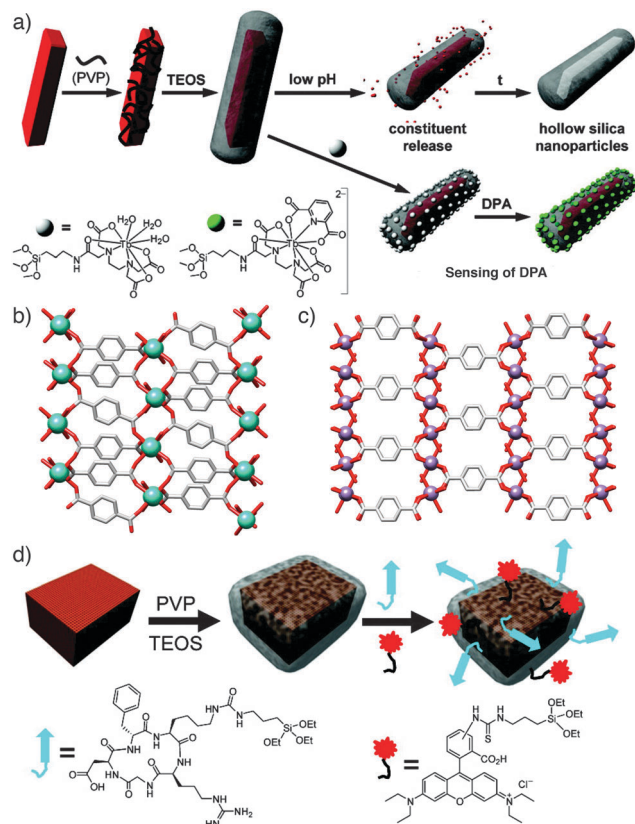
Fig. 8 (a) Synthetic scheme illustrating the sequential coating of [Ln(1,4-bdc)$_{1.5}$(H$_2$O)$_2$]$_n$ nanoparticles with PVP and silica, which allows either slow degradation and release or the further conjugation of terbium complexes to act as sensors. (b) The solid state structure of [Tb(1,4-bdc)$_{1.5}$(H$_2$O)$_2$]$_n$, redrawn from CCDC deposition QACTUJ. (c) The solid-state structure of [Mn(1,4-bdc)(H$_2$O)$_2$]$_n$, (CCDC deposition XUDSUK), which can be (d) coated in silica and further functionalised with cyclic c(RGDfK) peptide targeting agents and fluorescent Rhodamine B units. Reprinted (adapted) with permission from ref. 38 and 39. Copyright (2007 and 2008) American Chemical Society.

In these cases, the pre-treatment of the MOF nanoparticles with PVP protects the MOF against hydrolysis under the basic conditions required for silica deposition. A recent study by Zeng et al. has shown[41] that this protection can be achieved by basifying the deposition solution with coordinative species related to the MOF strut – 2-methylimidazole for ZIFs and sodium acetate for carboxylate-based MOFs, for example – and silica can be coated directly onto the surface of the MOF. Lin has also demonstrated[42] that if the MOF has metal–ligand bonds with excellent resistance to chemical reaction, for example, Zr carboxylate species, then silica can also be directly applied onto its surface. Phosphorescent MOFs, based on carboxylic acid functionalised [Ru(2,2′-bipy)$_3$] struts linked by Zr^{4+} cations, were directly silica coated and modified further with solubilising poly(ethylene glycol) (PEG) chains and PEG–anisamide conjugates. The anisamide-functionalised particles showed enhanced uptake into H460 human non-small-cell lung cancer cells, which was imaged by confocal microscopy. Similarly, iron carboxylate MOFs endowed with imaging moieties and prodrugs were

directly silica coated, and with the grafting of previously utilised c(RGDfK) targeting peptides to the silica, nanoparticles with high cytotoxicity against HT-29 cells resulted.[43]

Polymers alone are also effective MOF surface modification agents. As part of their investigations[44] into drug delivery from MOFs, Horcajada et al. decorated the surfaces of nanoparticles of a number of iron carboxylate MOFs with different polymers. Alkyl-modified chitosan, a dextran–fluorescein–biotin conjugate (M_W 10 000) and PEG (M_W 5000) were all post-synthetically coated on MOFs such as MIL-88A, an iron fumarate, and MIL-100, an iron trimesate, with coordination from active donor units of the polymers to the metal cations on the MOFs' surfaces ensuring attachment. MIL-88A could also be surface functionalised with PEG chains during synthesis in a coordination modulation process, by incorporating NH$_2$–PEG–OMe into the synthetic mixture. The PEGylated MOF nanoparticles showed near-neutral zeta potentials and also improved properties with respect to aggregation, both attractive features for drug delivery agents. Boyes et al. prepared[45] [Gd(1,4-bdc)$_{1.5}$(H$_2$O)$_2$]$_n$ nanoparticles and coated them with RAFT co-polymers (Fig. 9) which had been treated to ensure the trithiocarbonate RAFT agent was hydrolysed to form a thiol endgroup, posited to coordinate to Gd^{3+} cations on the surface of the MOF nanoparticle. Incorporating fluorescent Rhodamine B groups and targeting GRGDS-NH$_2$ peptides into the random co-polymer resulted in devices capable of targeted imaging of FITZ-HSA tumour cells, whilst post-synthetic tethering of methotrexate, an antineoplastic chemotherapeutic, to the polymer gave hybrids which showed dose-dependent treatment against the same cell line.

Lipids can also be used to coat MOF nanoparticles to enhance their intracellular uptake. Lin et al. have shown[46] that coordination polymers of various metals with anticancer drugs such as methotrexate can be surface modified with a lipid bilayer by simply stirring the nanoparticles with liposomes,
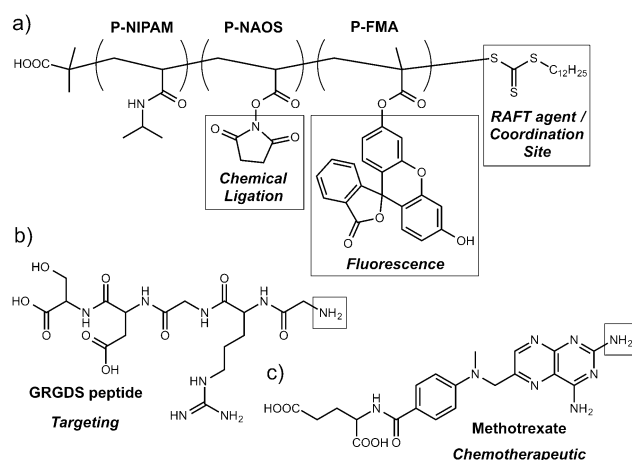

Fig. 9 (a) Chemical structure of the RAFT random co-polymer, comprised of N-isopropylacrylamide (NIPAM), N-acryloxysuccinimide (NAOS), and fluorescein-O-methacrylate (FMA) monomers, used to coat [Gd(1,4-bdc)$_{1.5}$(H$_2$O)$_2$]$_n$ nanoparticles. The activated NHS ester allows post-synthetic conjugation of (b) targeting GRGDS peptides and (c) methotrexate chemotherapeutic units through reaction with free amino groups.

which rearrange to encapsulate the nanoparticles. These lipid coated MOFs again show imaging and anticancer properties.

The surface coatings applied to these MOFs dramatically enhance their properties for biomedicinal applications, offering improved biostability and retention of cargoes, as well as the ability to graft further functionality, such as targeting units, to the outer surfaces of the material. The bulk surface treatments are likely to block the pores of the MOFs however, which may limit application in other areas, so it would be highly desirable to develop surface modification protocols which offered these enhanced properties while retaining access to the interior of the MOF material. A very recent example[47] succeeds in this aspect by coating particles of a MOF, UiO-66-NH$_2$ or [Zr$_6$O$_4$(OH)$_4$-(2-NH$_2$-1,4-bdc)$_6$]$_n$, with a porous polymer layer by carrying out the polymerisation on the surface of the MOF particles. The so-called microporous organic network was prepared by the Sonogashira coupling of tetra(4-ethynylphenyl)methane and linear diiodo-substituted aromatic units, and formed films of 8–30 nm thickness dependent on reaction ratios (Fig. 10).

The mode of attachment is presumably noncovalent, as (i) the amino groups of the MOF were available for post-synthetic modification after coating, and (ii) attempts to coat the analogous UiO-66-I, which could potentially form covalent bonds to the polymer through its reactive 2-I-1,4-bdc linker, formed poorer quality surface layers. The effect of coating a relatively hydrophilic MOF with a microporous hydrophobic polymer is to not only dramatically alter the wettability of the particles, but also enhance the uptake of hydrophobic toluene from water–toluene mixtures, an effect ascribed to the decreased wetting of the surface-modified MOF enhancing the toluene's access to

the pores. Porous polymers will no doubt prove highly effective surface modifying agents, to moderate the chemical environment around MOF pores without blocking access to them.

3.2 Surface modification by coordinative ligand or metal exchange

Solvent assisted linker exchange (SALE) has been extensively utilised to post-synthetically modify MOFs, with single crystal to single crystal transformations possible in which ligands can be partially or completely exchanged by soaking/heating MOF crystals in appropriate solutions of the exchanging species.[48] Confining exchange to the crystal surface, through steric effects or otherwise, can effectively control the surface chemistry of the MOF being addressed.

Coordinative surface ligand exchange has been successfully performed by the Kitagawa research group on two Zn-based MOFs of rectangular prism morphology: [Zn$_2$(1,4-ndc)$_2$(dabco)]$_n$ and [Zn$_2$(1,4-bdc)$_2$(dabco)]$_n$.[49] These tetragonal frameworks possess two crystal surface types which individually correspond to termination by carboxylate and dabco ligands. The group made use of coordinative interactions to impart a monolayer of boron dipyrromethene (BODIPY) molecules onto the four carboxylate [100] surfaces of the MOF crystals via coordinative ligand exchange (Fig. 11). Using a fluorescent dye such as BODIPY as the incoming ligand made it possible to probe and characterise the monolayer by confocal laser scanning microscopy (CLSM) which has been used extensively to monitor MOF surface chemistry. CLSM confirmed that the dye molecules selectively exchanged with the surface carboxylate ligands only, leaving the two dabco [001] surfaces of each crystal unmodified.
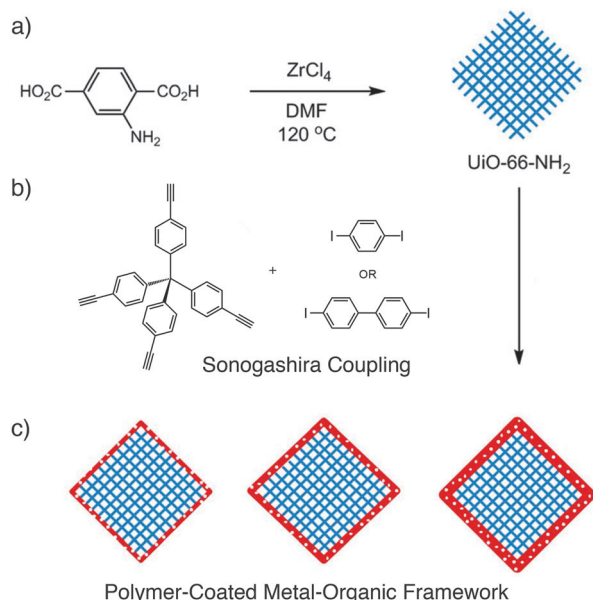

Fig. 10   (a) Synthesis of UiO-66-NH$_2$, which can (b) be coated with a microporous polymer through a Sonogashira reaction to yield (c) MOF particles with polymer coatings of varying thicknesses, depending on reaction conditions. Reprinted (adapted) with permission from ref. 47. Copyright (2014) American Chemical Society.
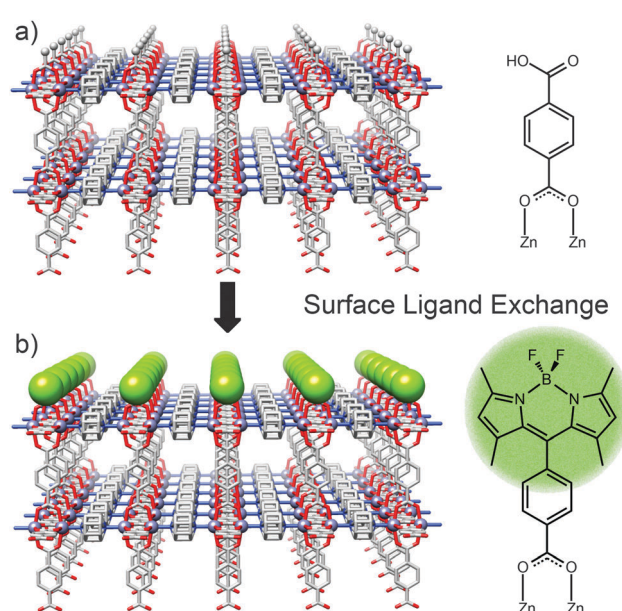

Fig. 11   Schematic diagram to demonstrate the exchange of surface ligands from (a) 1,4-benzenedicarboxylate units to (b) fluorescent BODIPY linkers in [Zn$_2$(1,4-bdc)$_2$(dabco)]$_n$. Ligand exchange only occurs at the carboxylate terminated [100] surfaces of the MOF as a result of the functional group complementarity with the BODIPY ligand.

In addition to selectivity for carboxylate ligands, the exchange process is confined to the surface by steric effects; compared to the carboxylate ligands, the BODIPY unit is much bulkier and cannot penetrate the MOF. Consequently, the dye adheres only to the surface of the MOF crystals, rather than permeating through the framework *via* the pores. The surface morphology pre- and post-modification was studied through the use of AFM (atomic force microscopy) which illustrated the uniformity of the BODIPY monolayer and confirmed its lack of aggregation.

The Kitagawa group further tested this PSM method by applying the same procedure to HKUST-1, where the [111] crystal surfaces are terminated by carboxylate groups in a comparable way to the previous Zn frameworks. In a change to the experimental procedure, the HKUST-1 protocol required a higher temperature and longer time interval than was needed for the Zn frameworks. These more forcing reaction conditions were brought about by the higher relative strength of Cu–carboxylate coordination bonds compared to Zn–carboxylate coordination bonds. Despite these conditions, complete surface coverage of HKUST-1 crystals was observed, while fluorescence spectroscopy confirmed that the BODIPY ligands did not enter the pores of the framework, demonstrating the formation of a coordinative monolayer on MOFs with carboxylate surfaces.

Similar behavior has been observed with ZIFs. Granick *et al.* showed[34,35] by fluorescence imaging that surface ligands of ZIF-8 could be exchanged with an imidazole-linked BODIPY dye (Fig. 12a and b), with the ZIF-8 particle size in this case previously controlled by coordination modulation. This combined approach could effectively allow control of size and surface chemistry of MOFs in a two-step procedure.

Yang *et al.* subsequently demonstrated[50] that controlling the chemistry of the surface ligands of ZIF-8 could impact its materials properties (Fig. 12c). Exchanging the surface ligands of ZIF-8 from 2-methylimidazole to the more hydrophobic 5,6-dimethylbenzimidazole (DMBIM), as characterised by FTIR

and Raman spectroscopies, significantly enhanced the stability of the surface modified ZIF-8 towards hydrolysis, presumably as a result of the more hydrophobic DMBIM outer layer protecting the ZIF from attack by water. This stabilisation effect can be extended to other ZIFs, while the hydrophobicity of the surface also influences absorption and separation of guests – tentative signs that surface modification of MOFs could have significant impact on host–guest chemistry by moderating the chemical environment around pore openings.

Whilst surface ligand exchange can be limited to the surface of a MOF crystal by the steric bulk of the added functionality, surface metal exchange is much harder to control. Lah *et al.* have demonstrated[51] that both partial and complete transmetallation can be induced in pillared MOFs, with the extent of metal exchange and so depth of penetration of the new metal dependent (Fig. 13a) on the time of the experiment and the kinetic properties of the metal cations in question. In the MOF $[Co_6(1,3,5\text{-btb})_4(4,4'\text{-bipy})_3]_n$ (btb = benzenetribenzoate), even partial surface exchange of Co(II) for Ni(II) induces a structural change across the bulk framework, dramatically enhancing the porosity of even partially transmetallated MOFs.

Hupp *et al.* have also demonstrated[52] that, when metal cations form an intrinsic part of the linker, they can be selectively removed at the MOF surface or near surface. MOFs comprised of a tetracarboxylic acid strut and a manganese-salen based pillar linked by Zn^{2+} cations could be demetallated by addition of H_2O_2. However, preloading the pores of the MOF with a water-immiscible solvent, $CHCl_3$, prevented penetration of aqueous H_2O_2 into the MOF pores and so demetallation could be limited to the surface only, causing a change in the catalytic properties of the material.

Much stricter control of the metal cations at a MOF surface can be achieved by a combination of the previous approaches. Hupp *et al.* have shown[53] that limiting ligand exchange to the surface of a MOF using steric effects, followed by selectively binding metal cations to these surface ligands, can selectively
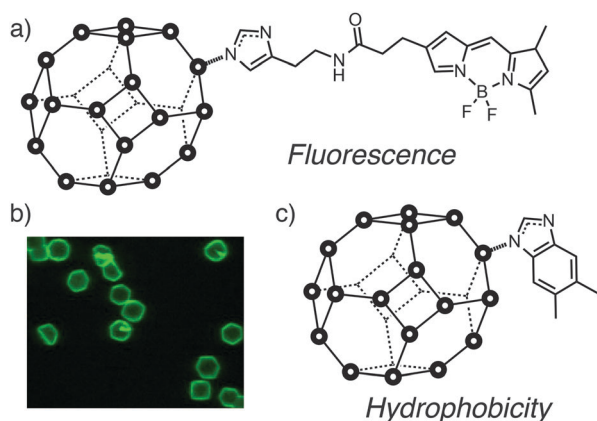

Fig. 12 Exchange of surface ligands of ZIF-8 allows attachment of (a) fluorescent BODIPY dyes to (b) visualise the surface ligand exchange by fluorescence microscopy, while incorporation of (c) hydrophobic surface functionality such as 5,6-dimethylbenzimidazole significantly increases the hydrolytic stability of ZIF-8. Part (b) reprinted (adapted) with permission from ref. 35. Copyright (2013) American Chemical Society.
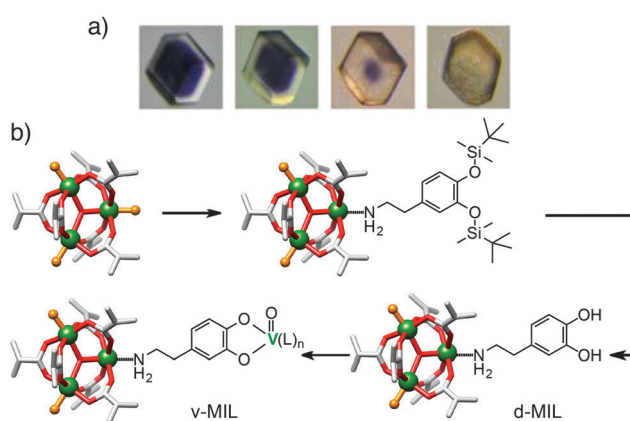

Fig. 13 (a) Photographs of metal cation exchange in $[Co_6(1,3,5\text{-btb})_4(4,4'\text{-bipy})_3]_n$, occurring from the surface of the crystal inwards. Reprinted (adapted) with permission from ref. 51. Copyright (2012) American Chemical Society. (b) Scheme showing coordination of bulky TBDMS-protected dopamine to the Cr^{3+} cations of the SBUs at the surface of MIL-101(Cr) only, which can then be deprotected and vanadylated.

surface-modify a MOF with desired metal cations. The large-pore MOF MIL-101(Cr), which consists of $[Cr_3O(X)(H_2O)_2L_6]$ octahedral SBUs, where L = 1,4-bdc and X = a monoanionic counterion, was synthesised and heated to remove the two aqua ligands from each trimeric unit, providing coordination sites for the surface functionality. Dopamine units could subsequently be added *via* coordination of the amino moiety to the Cr^{3+} cations, leaving its catechol group available for further coordination. To ensure the dopamine units were coordinated only at the surface, it was necessary to protect their hydroxyl units with *tert*-butyl-dimethylsilyl (TBDMS) groups, whose steric bulk prevented the penetration of the dopamine units into the pores of the MOF, forming the surface modified species the authors termed d-MIL (Fig. 13b). Once grafted onto the MIL-101 surface, these dopamine ligands can be deprotected prior to coordination to vanadyl groups through reaction with $VO(acac)_2$, to form the vanadium substituted MOF, termed v-MIL. An alternative application of the protected d-MIL framework is in the preparation of a core–shell MOF. The protected d-MIL structure can be treated with an amine of size small enough to enter the pores for internal pore surface functionalisation, while the outer TBDMS-dopamine ligands would remain in their position on the exterior of the MOF.

Following its successful production, the effectiveness of v-MIL as a catalyst for thioanisole oxidation was examined. Compared to $VO(acac)_2$ when used as a homogeneous catalyst for this process, conversion of the thioether to the sulfoxide was slower, but conversion of the sulfoxide to the subsequent sulfone occurred at a similar rate. Catalyst recovery and recycling was also proven to be efficient, with good yields of oxidised thioanisole reported from recycled v-MIL. Use of this surface-modified MOF as a catalyst presents an advantage over homogeneous catalysts in the form of coordinative unsaturation of the chelated cation; this situation would not arise in a homogeneous catalyst.

Overall, ligand or metal exchange at the MOF surface is a simple way to introduce functionality to already synthesised MOFs. Limiting the exchange to the MOF surface is the challenging step, with steric hindrance working well for ligand exchange, but metal exchange is difficult to control and can lead[54] to core–shell structures (see Section 4.1). The few examples of surface ligand exchange illustrate its power in altering both stability and uptake of MOF particles – more complex examples will no doubt follow, likely in concert with other methods of post-synthetic modification.

3.3 Covalent surface modification

Post-synthetic modification of MOFs by covalent methodology is well established, with numerous chemical transformations capable of facilitating bulk functionalisation.[36] There are only a small number of examples where covalent modification has been limited to the surface of a MOF, with two main strategies: (i) adding functionality that is too large to fit into the pores of the MOF, and (ii) selectively unmasking reactive moieties at the surface of the MOF only, with subsequent surface-only modification. The former limits the scope of surface modification to either MOFs with small pores or surface decoration with large bulky units, and so few examples exist.
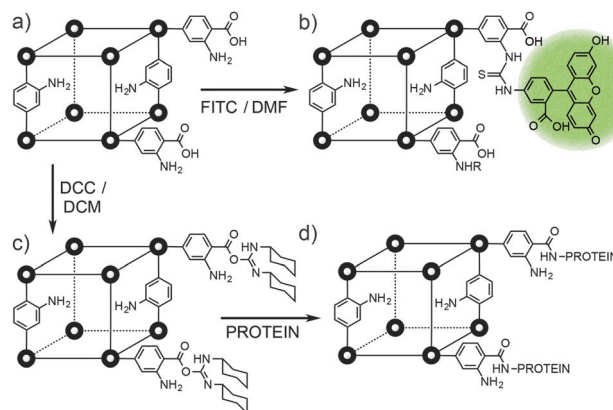

Fig. 14 (a) Schematic of IRMOF-3, which can be surface functionalised (b) at its amino groups, for example through bulky fluorescent FITC tagging, and at its terminal surface carboxyl units by (c) DCC activation and (d) subsequent protein conjugation.

Cohen *et al.* described, during a study[55] of the post-synthetic modification with anhydrides of IRMOF-3, $[Zn_4O(2-NH_2-1,4-bdc)_6]_n$, that reaction of the amino moieties of the MOFs with long chain dialkyl anhydrides produced materials that were highly hydrophobic – despite low overall conversions – and postulated that modification was limited to near the surfaces of the MOF crystals. Fischer and Metzler-Nolte provided evidence of surface-selective PSM, when crystals of IRMOF-3 (Fig. 14a and b) were reacted[56] in DMF at room temperature with the well-known biological tag Fluorescein IsoThioCyanate (FITC) for one day. Confocal fluorescence microscopy showed attachment of the fluorescent dye only at the surface, with UHV-FT infrared spectroscopy showing the formation of the thiourea linkage on the surface of the MOF and ESI-MS of digested samples giving m/z peaks for the covalently linked product of the reaction between 2-NH$_2$-1,4-bdc and FITC. Control reactions with MOF-5, the isoreticular analogue which has no NH_2 groups for covalent functionalisation, showed no reaction or fluorescence, as expected.

It is even possible to append molecules as large as proteins to the exteriors of MOFs. Park and Huh demonstrated[57] that the free carboxyl units of linkers at the surfaces of MOFs can be activated using carbodiimide coupling agents to facilitate bioconjugation with different proteins. Three MOFs, the one dimensional $[In(1,4-pda)_2(NEt_2H_2)]_n$ (pda = phenylenediacetate), the two dimensional $[Zn(bpydc)(H_2O)_2]_n$ (bpydc = 2,2′-bipyridine-5,5′-dicarboxylate) and the three dimensional IRMOF-3, were all activated towards bioconjugation with 1-ethyl-3-(3-dimethylaminopropyl) carbodiimide (EDC) or dicyclohexyl carbodiimide (DCC). Protein surface attachment (Fig. 14c), carried out in aqueous buffer, was visualised initially by using enhanced green fluorescent protein (EGFP), which was unambiguously identified on the surfaces of the MOFs by CLSM. A catalytic enzyme, *Candida antarctica* lipase B, was also attached to the MOFs' surfaces, in yields of approximately 0.1–0.2 mg of protein per gram of MOF. The catalytic activity and enantioselectivity of the protein in a transesterification reaction was retained, and it was also possible to attach a second EGFP protein to the same MOF.

Similar size-based reactivity trends have been postulated by Sada *et al.*, with an azide functionalised framework thought to
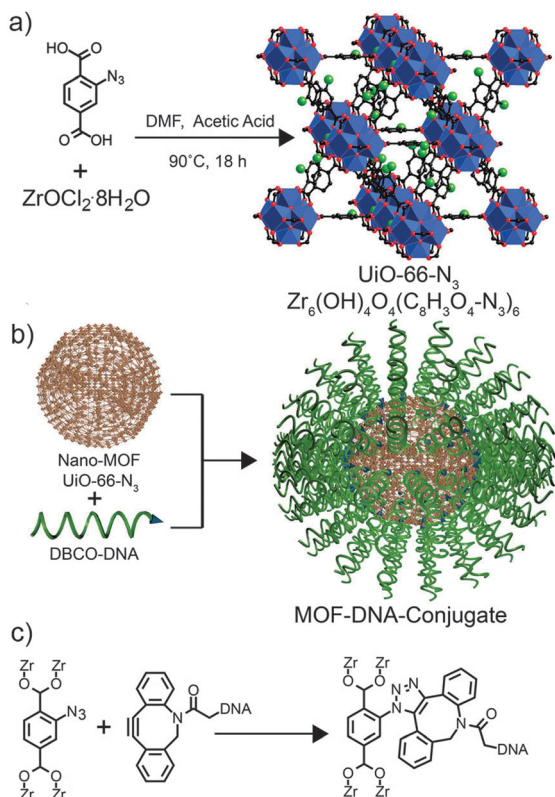
Fig. 15 (a) Synthesis of UiO-66-N$_3$. (b) Schematic surface attachment of oligonucleotides to UiO-66-N$_3$ nanoparticles. (c) Chemical structure of the strain-promoted click reaction between 2-N$_3$-1,4-bdc ligands of the MOF and DBCO functionalised DNA. Reprinted (adapted) with permission from ref. 59. Copyright (2012) American Chemical Society.

was a triclinic Zn-based framework with 2,6-ndc ligands and 1,2-bpe-based pillars, of which the latter possess trimethylsilyl (TMS) protected acetylene groups; selective surface deprotection of the alkynes would allow for control of the location of a subsequent CuAAC reaction with ethidium bromide monoazide (EBM) to impart surface fluorescence. Surface selective deprotection of the reactive alkyne unit was achieved by the use of a F$^-$ ion source with a bulky countercation, tetra-n-butylammonium (TBA). The TBAF was too large to diffuse throughout the porous material, and less than 0.8% of the alkyne groups were deprotected. Removal of the TMS group by F$^-$ was verified by matrix-assisted laser desorption ionisation time-of-flight (MALDI-TOF) mass spectrometry and ^{1}H NMR spectroscopy, confirming the selectivity of the surface deprotection, allowing EBM, a fluorescent dye, to be conjugated to the MOF's deprotected surfaces. MALDI-TOF mass spectrometry and confocal fluorescence microscopy proved that the EBM ligands were bound solely to the surface of the MOF *via* a covalent bond with the terminal acetylenes, while control reactions between unfunctionalised [Zn$_2$(2,6-ndc)$_2$(1,2-bpe)]$_n$ and EBM resulted in products which were not fluorescent. Further analysis of the surface-clicked MOF provided evidence that its interior structure showed little variation from that of the original, unmodified framework.

Following the successful surface deprotection and click functionalisation of this Zn-based MOF, Hupp and co-workers treated the surface-deprotected MOF with an azide of poly(ethylene glycol), with PEG conjugation resulting in the MOF presenting a hydrophilic surface. The unmodified, surface-protected MOF was observed to repel water, while the deprotected material's newly-installed hydrophilicity was apparent when tested with drops of coloured water, which penetrated the gaps between packed crystals of the deprotected MOF. In contrast, water did not filter through crystals of the surface-protected MOF and droplets remained on the surface of the material (Fig. 16a and b).

An analogous Zn MOF with extended 1,2,4,5-tcpb ligands (tcpb = tetrakis(4-carboxyphenyl)benzene) and the same TMS-alkyne-1,2-bpe pillar was also synthesised (Fig. 16c). To ensure that only the framework surface was deprotected, this larger pore MOF underwent solvent exchange with chloroform and was subsequently treated with an aqueous KF solution, which is immiscible with the CHCl$_3$ and so did not permeate the chloroform-filled pores of the framework. After selective surface functionalisation of the deprotected alkynes through a CuAAC reaction, it was found[61] that the larger pore sizes allowed a second post-synthetic modification step to be carried out in the remainder of the bulk MOF. Diffusing THF solutions of tetraethylammonium fluoride into the surface modified MOF deprotected the alkyne functionalities in the inner area of the particles, thus allowing a second distinct CuAAC reaction to yield core–shell post-synthetically modified materials (Fig. 16d).

Sada and co-workers utilised[62] an alternative surface-selective deprotection reaction to unmask amino groups capable of further reaction. An IRMOF-9 derivative comprised of Zn$_4$O clusters linked by biphenyl dicarboxylic struts with two azido-methylene substituents was prepared, and the azide units selectively reduced at the crystal surface (Fig. 17a). The Staudinger

only undergo surface modification, through the copper catalyzed azide–alkyne cycloaddition (CuAAC) "click" reaction, with long-chain alkynes due to steric effects, but further evidence is required to confirm this.[58] Mirkin *et al.* have recently demonstrated[59] that surface functionalisation of MOFs by strain-promoted azide–alkyne cycloaddition is possible when using large oligonucleotide sequences as surface ligands. An azide functionalised MOF, UiO-66-N$_3$ [Zr$_6$O$_4$(OH)$_4$(2-N$_3$-1,4-bdc)$_6$]$_n$, was prepared in nanoparticulate form over a range of sizes, from 14–500 nm, and reacted with dibenzylcyclooctyne (DBCO) functionalised DNA sequences in aqueous conditions (Fig. 15), with slow addition of NaCl used to reduce electrostatic interaction between oligonucleotide strands and promote higher surface coverage. Various oligonucleotides with lengths over 20 base pairs were attached to the surfaces of the MOF nanoparticles, and were found to alter their zeta potentials and aggregation behavior, as well as dramatically enhancing their cell uptake. With fluorescent oligonucleotides also attachable and used to monitor surface coverage, these final cell uptake results have significant implications in drug delivery and imaging using surface modified MOF nanoparticles.

Alternative covalent surface modification methods have involved the selective unmasking of functionality only at the surfaces of MOF crystals. Hupp and co-workers investigated[60] post-synthetic deprotection of a MOF exterior followed by covalent reaction *via* CuAAC "click" chemistry. The MOF in question
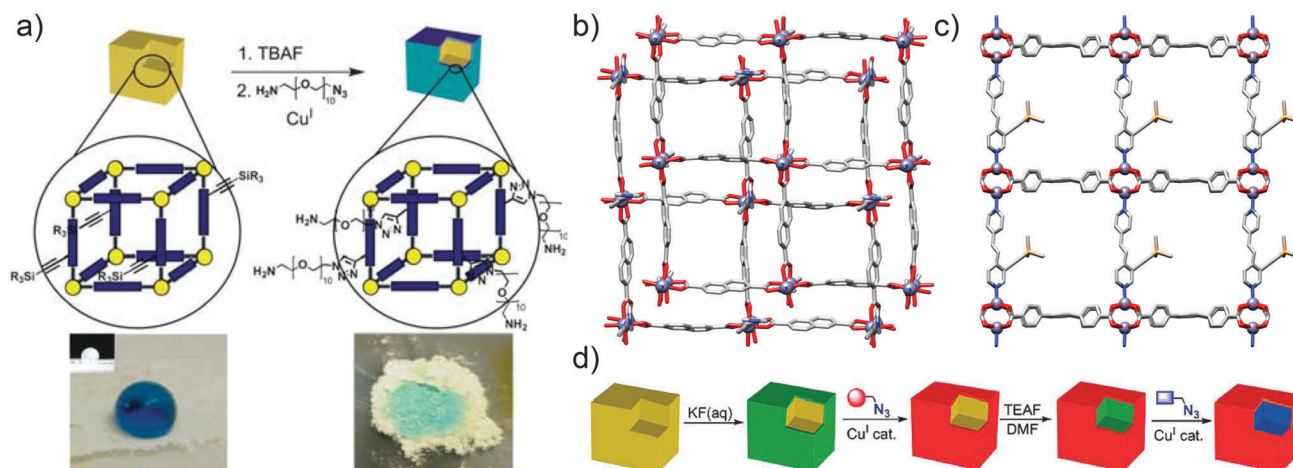
Fig. 16 (a) Selective surface deprotection of alkyne units of $[Zn_2(2,6\text{-ndc})_2(\text{TMS-alkyne-1,2-bpe})]_n$ allows surface modification with hydrophilic PEG groups, significantly changing the wettability of the MOF. Reproduced from ref. 60 with permission from The Royal Society of Chemistry. (b) Crystal structure of the underlying $[Zn_2(2,6\text{-ndc})_2(1,2\text{-bpe})]_n$ framework, redrawn from CCDC deposition PITREQ. (c) Crystal structure of the TMS-alkyne substituted $[Zn_2(1,2,4,5\text{-tcbp})(\text{TMS-alkyne-1,2-bpe})]_n$, redrawn from CCDC deposition LURGEL, which can (d) be surface modified through selective deprotection of the alkyne groups, and subsequently functionalised throughout the remainder of the material to produce a core–shell functionalised species. Reprinted (adapted) with permission from ref. 61. Copyright (2009) American Chemical Society.

reduction typically uses as a reducing agent triphenylphosphine, whose relatively large size is ideal for ensuring selective surface PSM as it cannot penetrate the pores of the MOF. ^{1}H NMR spectroscopy confirmed only 1.3 mol% of the azides were converted to amines, and their reactivity was tested by conjugation with a fluorescent dye containing an *N*-hydroxysuccinimide (NHS) activated ester moiety. On probing the crystals with CLSM, strong fluorescence was observed towards the outside of the framework, while scanning deeper within the crystal showed that the fluorescence was much weaker (Fig. 17b). The decrease in fluorescence implies the generation of a surface modified MOF structure, where the core is made up of unmodified azide struts and the shell consisting of the newly-functionalised amide struts, although the large fluorescent dye may be too large to diffuse into the interior of the MOF.

A number of successful strategies have been pioneered to post-synthetically modify MOF surfaces, each with their own advantages and disadvantages. Click reactions in particular have been found to be successful when performing PSM on MOFs as only mild conditions are needed and no side reactions occur.[63] Surface exchange processes have also proven very useful; a combination of surface exchange and covalent modification would be expected as a subsequent next step in post-synthetic surface modification of MOFs.

4. Epitaxial growth of MOF hybrids

An alternative method to address the surfaces of MOF particles is to take previously synthesised MOFs and epitaxially grow a second, distinct MOF upon its surface, with the second crystalline component perfectly in register with the first. This combination of post-synthetic modification and *in situ* MOF surface modification has been successfully demonstrated both on bulk MOF samples, to yield core–shell hybrids, and on thin
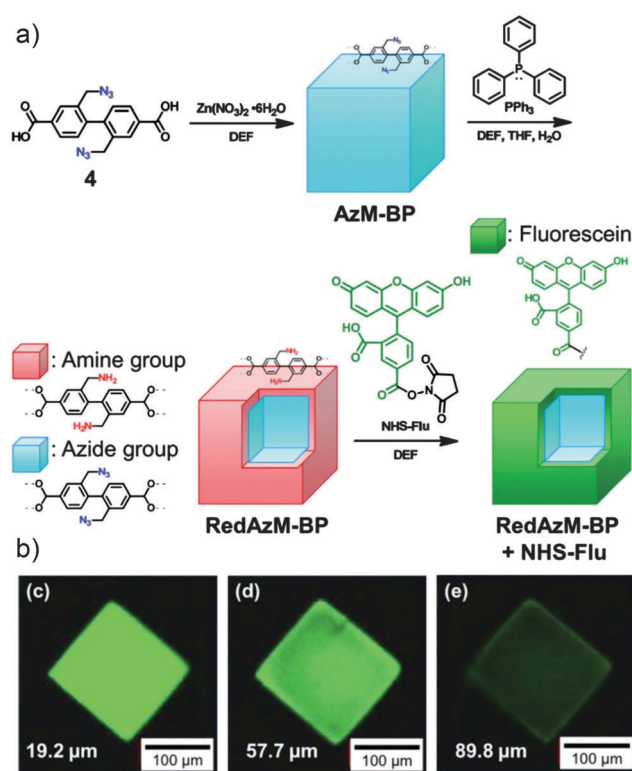

Fig. 17 (a) Synthetic scheme for surface functionalisation of an azide substituted MOF through a size-selective, surface limited Staudinger reduction to amino groups, which are subsequently reacted with NHS-activated fluorescein tags. (b) Confocal fluorescence microscopy shows the fluorescence, and so location, of the fluorescein units is confined to the surface of the MOF. Adapted from ref. 62 with permission from The Royal Society of Chemistry.

films, giving layer-by-layer surface modified films. The ability to combine different MOFs into one hybrid material or film, as

well as further functionalisation by selective post-synthetic modifications to specific components, opens up the possibility of modular devices with multiple properties, such as conjugated small molecule catalysis and purification units or enhanced sorption and separation of desirable analytes.

4.1 Core–shell hybrid MOFs

Large-scale growth of one MOF on another produces core–shell species that have been variously described as hybrid- or hetero-MOFs, MOF@MOFs and MOF-on-MOF materials. Lattice matching is usually required for MOF-on-MOF growth; that is, the metal SBUs of the 'core' layer must align with those of the 'shell' layer, so most materials comprise of MOFs with similar crystallographic parameters.

The Kitagawa research group demonstrated[64] the MOF-on-MOF self-assembly method in the synthesis of $[Cu_2(1,4\text{-}ndc)_2(dabco)]_n$ on a substrate of the Zn equivalent, $[Zn_2(1,4\text{-}ndc)_2(dabco)]_n$. These two frameworks were chosen to illustrate proof-of-principle MOF-on-MOF growth due to their similarity and robustness; the structures remain tetragonal upon variation of the metals and both types of ligand, meeting the lattice-matching criteria required for MOF-on-MOF synthesis. The Cu analogue of this MOF can only be obtained as a microcrystalline powder, whereas the Zn analogue can be solvothermally synthesised as cubic crystals. The Zn crystals were placed into a toluene–methanol solution of $CuSO_4 \cdot 5H_2O$, 1,4-ndc and dabco, and green crystals resulted (Fig. 18a); this difference in colour indicates that the Cu-based MOF has grown on the Zn framework surface and hence the crystals are core–shell hybrids. X-Ray diffraction studies provided evidence for epitaxial growth of the Cu shell on the Zn core and also proved that the hybrid crystals were indeed single crystals. The core Zn-MOF templates the growth of the shell framework into crystals of sizes not normally achievable by conventional solvothermal methods, suggesting that control of MOF surface chemistry could facilitate the templated self-assembly of otherwise unattainable MOFs through controlled seeding and epitaxial growth.

In contrast to this initial example of heterometallic core–shell materials, Matzger et al. demonstrated[65] the ability to produce so-called MOF@MOF species where the metal remains constant and the ligands are varied, by utilising a range of isoreticular zinc terephthalates of composition $[Zn_4OL_6]_n$. After solvothermally synthesising crystals of the first MOF, these crystals were exposed to a second solvothermal step using an alternative ligand, resulting in MOF-on-MOF growth. Having successfully prepared a core–shell structure of IRMOF-3 (2-NH2-1,4-bdc linkers) grown epitaxially on MOF-5 (1,4-bdc linkers), a further layer of MOF-5 was deposited on the outer IRMOF-3 layer to create a "core–shell–shell" MOF. The overall tri-layer MOF obtained was therefore termed MOF-5@IRMOF-3@MOF-5. Provided that the lattices align sufficiently, the deposition of even more layers is possible for the production of multi-layer MOFs. In fact, it is possible to form IRMOF-3@MOF-5@IRMOF-3; the 'inverse' of the previous tri-layer MOF (Fig. 18b). To reflect this, Matzger and co-workers dubbed these structures 'Matryoshka'
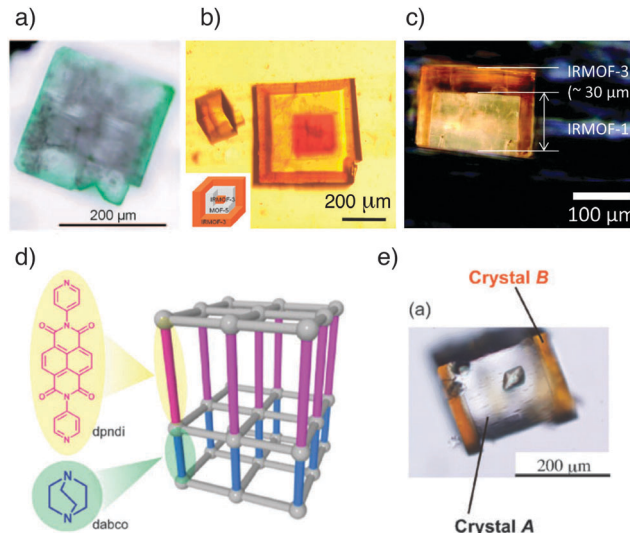

Fig. 18 Images of various core–shell MOFs from epitaxial crystal growth. (a) A binary system composed of green $[Cu_2(1,4\text{-}ndc)_2(dabco)]_n$ on colourless $[Zn_2(1,4\text{-}ndc)_2(dabco)]_n$. Reprinted (adapted) with permission from ref. 64. Copyright (2009) John Wiley and Sons. (b) A triple layer system of IRMOF-3@MOF-5@IRMOF-3. Adapted from ref. 65 with permission from The Royal Society of Chemistry. (c) A so called Janus hybrid, where the coverage of MOF-5 (also known as IRMOF-1) by IRMOF-3 is limited by adhesion of the base of the core crystal to a surface. Reprinted (adapted) with permission from ref. 66. Copyright (2010) American Chemical Society. (d) Schematic showing face-selective epitaxial growth in a pillared MOF. (e) Face-selective epitaxial growth of orange $[Zn_2(1,4\text{-}ndc)_2(dpndi)]_n$ on the [001] faces only of colourless $[Zn_2(1,4\text{-}ndc)_2(dabco)]_n$. (d) and (e) adapted from ref. 68 with permission from The Royal Society of Chemistry.

MOFs owing to their resemblance to Russian dolls. Again, a templating effect is observed; when growing MOF-5 on a seed crystal of IRMOF-3, pristine non-interpenetrated MOF-5 forms on the surface, as opposed to the phase impure material that results from non-templated synthesis under identical conditions.

Jeong et al. reported similar results[66] when growing core–shell hybrids of IRMOF-3 and MOF-5, managing to prepare hybrid membranes, but it was found that addition of a base to the synthesis was required to ensure hybrid growth. Szilágyi reported[67] the assembly of core–shell materials comprised of MOF-5 and IRMOF-2, which has 2-bromoterephthalate as ligand, and found that strain led to collapse of the core MOF after complete coating by the outer shell. So-called Janus particles (Fig. 18c), with only partial coating of the core due to attachment of crystals to glass surfaces, did not show core collapse. Further work is required to examine the effect of surface modifying MOFs in this way.

As epitaxial growth is itself a surface-related technique, it is reasonable that it might be limited to particular types of surface in an anisotropic crystal. The Kitagawa research group achieved surface-selective[68] epitaxial growth with the $[Zn_2(1,4\text{-}ndc)_2\text{-}(dabco)]_n$ tetragonal framework, which lends itself well to surface-selective techniques on account of its multi-ligand character and hence different surface types. The [001] dabco-terminated surfaces were used as the substrate for growth of a similar MOF, $[Zn_2(1,4\text{-}ndc)_2(dpndi)]_n$ (dpndi = N,N′-di(4-pyridyl)-1,4,5,8-naphthalenetetracarboxydiimide). Crystals of the original

dabco framework were exposed to a DMF solution of $Zn(NO_3)_2\cdot 6H_2O$, 1,4-ndc and dpndi ligands under solvothermal conditions, but epitaxial growth was only observed on the [001] faces (Fig. 18d and e). The large difference in length between the dabco and dpndi ligands results in dramatic lattice-mismatching along the [100] faces and so the secondary framework cannot grow on the core in these directions.

Core–shell hybrid MOFs have been used to demonstrate the important principle that surface modification of a MOF can significantly affect its bulk properties. Kitagawa *et al.* prepared[69] a hybrid comprised of a $[Zn_2(1,4\text{-bdc})_2(\text{dabco})]_n$ core coated with a $[Zn_2(9,10\text{-adc})_2(\text{dabco})]_n$ shell (adc = anthracene-dicarboxylate). The steric bulk of the 9,10-adc ligand means that $[Zn_2(9,10\text{-adc})_2(\text{dabco})]_n$ can selectively absorb cetane (*n*-hexadecane) *versus* the isomeric isocetane (2,4,4,6,8,8-heptamethylnonane) as a result of its small pore openings excluding the bulkier isomer (Fig. 19a and b). $[Zn_2(1,4\text{-bdc})_2(\text{dabco})]_n$ has a higher storage capacity for cetane, as a result of its larger pore volume, but also displays poor selectivity for absorption of these two isomers. The core–shell hybrid, however, combines the selectivity of the outer framework with the increased storage capacity of the inner, and so the material exhibits excellent selectivity for absorption of cetane (and exclusion of isocetane) through the outer, restricted pore windows *and* increased storage capacity in the more spacious inner framework (Fig. 19c). Surface modification of the MOF, through core–shell hybrid formation, has produced a material with properties that cannot be achieved by either unfunctionalised MOF alone.

It is also possible to post-synthetically modify core–shell MOFs selectively on the outer shell. The $[Zn_2(9,10\text{-adc})_2(\text{dabco})]_n$ framework was coated[70] with the amino-functionalised $[Zn_2(2\text{-NH}_2\text{-}1,4\text{-bdc})_2(\text{dabco})]_n$ material, and reaction of the amine groups with succinic anhydride proceeded only in the shell region, with approximately 50% conversion. As the reaction generates free carboxylic acid moieties within the pores of the shell, it was found that selective absorption of *N,N'*dimethylaniline over benzene could be achieved as a result of the interaction between the carboxyl and amino units of the host and guest, respectively.

Rosi *et al.* recently described[71] both enhanced uptake selectivity and stability in a core–shell hybrid involving bio-MOF-11 and bio-MOF-14 (Fig. 20a), which have the compositions $[Co_2(\text{ad})_2(CH_3CO_2)_2]_n$ and $[Co_2(\text{ad})_2(n\text{-C}_4\text{H}_9\text{CO}_2)_2]_n$, respectively (ad = adeninate). The increased hydrophobicity of bio-MOF-14 affords it much greater water stability than bio-MOF-11, and it also offers greater CO_2/N_2 absorption selectivity, albeit with a lower capacity. bio-MOF-11 has a much higher capacity for CO_2 but with lower selectivity, however, attempts to create a core–shell architecture to combine the properties of pure bio-MOF-11 and bio-MOF-14 were unsuccessful, likely as a result of the crystallographic parameters of the two being too different and lattice-mismatching occurring. When the inner shell comprised a solid solution of bio-MOF-11/14, with a random homogenous
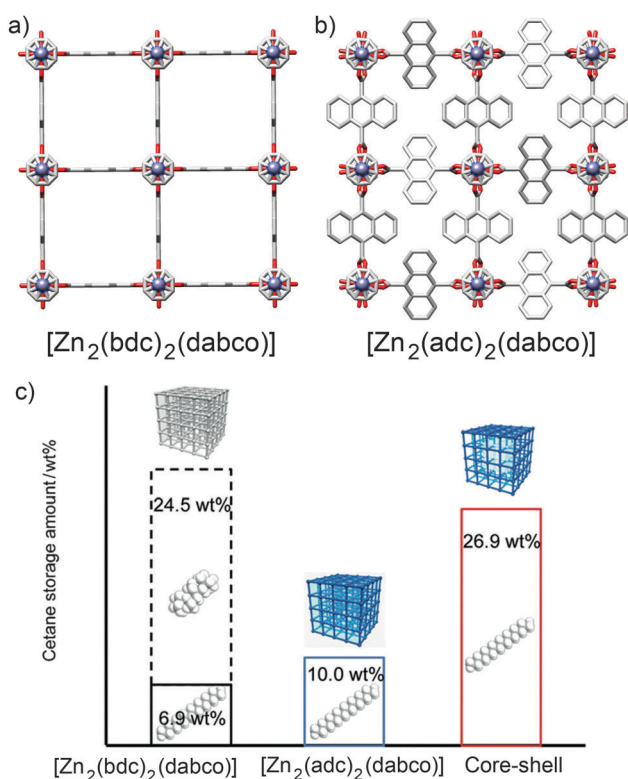

Fig. 19 Crystal structures of (a) $[Zn_2(1,4\text{-bdc})_2(\text{dabco})]_n$ and (b) $[Zn_2(9,10\text{-adc})_2(\text{dabco})]_n$, showing the considerable steric bulk in the pores of the latter compared to the former. Redrawn from CCDC depositions WAFKEU02 and IYATEI, respectively. (c) $[Zn_2(1,4\text{-bdc})_2(\text{dabco})]_n$ has a large capacity but unselective sorption of cetane isomers while $[Zn_2(9,10\text{-adc})_2(\text{dabco})]_n$ exhibits low but selective storage of cetane only. A core–shell hybrid of the pair combines both properties to give selective cetane absorption through the outer layer and enhanced storage capacities in the inner layer. Reprinted (adapted) with permission from ref. 69. Copyright (2011) John Wiley and Sons.
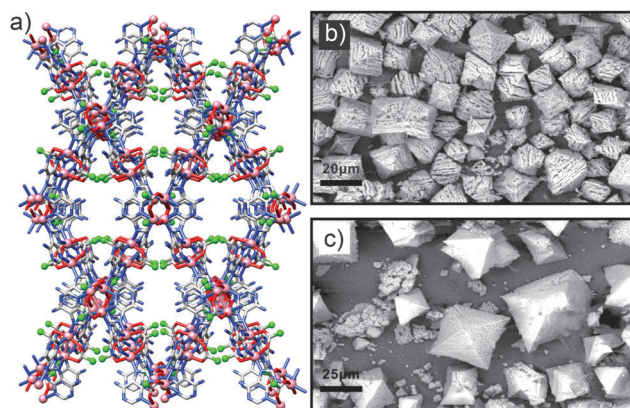

Fig. 20 (a) The crystal structure of bio-MOF-11, with the terminal carbon atoms of the acetate anions shown as green spheres (redrawn from CCDC deposition YUVSUE). Replacement of these acetate anions with *n*-butanoate ones gives the more hydrophobic bio-MOF-14. (b) SEM image of bio-MOF-11/14 core crystals after exposure to water for 24 h, showing significant damage, in contrast to (c) SEM images of the same core MOF coated with a shell of bio-MOF-14, which is considerably more stable to hydrolysis and confers this protection to the whole hybrid. Parts (b) and (c) reprinted (adapted) with permission from ref. 71. Copyright (2013) American Chemical Society.

distribution of the different monocarboxylate units, solvo-thermal surface growth of bio-MOF-14 could be achieved to form the core–shell hybrid. Compared to pure bio-MOF-14, the hybrid exhibited 30% greater uptake of CO_2 with excellent selectivity, and the hybrid was also found to be considerably more stable towards hydrolysis than the bio-MOF-11/14 core alone (Fig. 20b and c).

These examples confirm that strict control over surface chemistry of MOFs can engender them with enhanced properties, with some hybrids exhibiting properties unavailable to their individual components. However, it is difficult to control the thickness of the various surface layers using the solvothermal core–shell approach, and so other techniques have been developed.

4.2 Epitaxial MOF thin films

MOF thin films can be prepared by a number of methods and have found application in sensing, catalysis and purification.[72] Layer-by-layer (LBL) deposition[73] offers fine control over the thickness and composition of films, and is usually achieved by stepwise growth of individual layers of MOFs on surfaces covered with appropriate functionality, for example, gold wafers covered with a self-assembled monolayer projecting upwards pyridine units for metal coordination and thin film templation. Combining LBL deposition with liquid phase epitaxial growth offers the ability to selectively address surfaces of MOF thin films and prepare hybrid films with the potential for further post-synthetic functionalisation.

Kitagawa and Fischer first demonstrated[74] the ability to prepare hybrid systems in thin films, accomplishing the LBL deposition of $[Zn_2(1,4\text{-ndc})_2(dabco)]_n$ onto a surface mounted Cu analogue. In a typical experiment, a surface anchored MOF film is grown upon a gold substrate covered with a self-assembled monolayer (SAM) of 4-(4-pyridyl)phenylmethane-thiol (PPMT). Alternatively introducing an ethanolic solution of the metal as its acetate salt and an ethanolic solution of ligand(s) to link the metals, with intermediate washing steps, builds up the MOF film one layer at a time. The pyridine units mimic the dabco ligands and template the crystallisation of the MOF in the [001] direction, which can be confirmed by out-of-plane X-ray diffraction analysis that typically shows only the [001] and [002] reflections at appropriate 2θ angles for the MOF in question. The stepwise growth can also be monitored by surface plasmon resonance spectroscopy. A thin film consisting of 60 layers of $[Cu_2(1,4\text{-ndc})_2(dabco)]_n$ was deposited by this method, and simply changing the metal source to zinc acetate allowed a further 60 layers of $[Zn_2(1,4\text{-ndc})_2(dabco)]_n$ to be grown epitaxially upon the Cu base (Fig. 21).

LBL epitaxial growth offers exquisite control over the surface chemistry of the base film, with surface layers of atomic precision possible, but the technique is somewhat time-consuming and tricky to scale up in comparison to regular solvothermal synthesis. Applications in advanced separation techniques such as capillary gas chromatography columns are envisaged.

A combination of LBL liquid phase epitaxy and covalent PSM was employed[75] by Fischer and co-workers in order to achieve surface-selective functionalisation of thin films. A thin film of
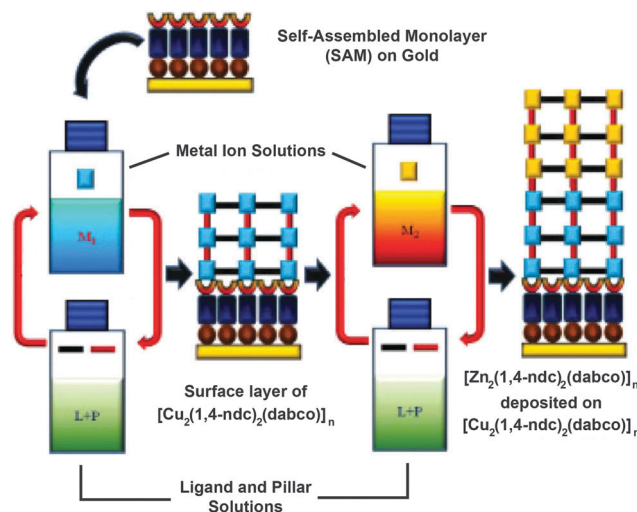

Fig. 21 Mechanism for the preparation of an epitaxial MOF thin film of $[Zn_2(1,4\text{-ndc})_2(dabco)]_n$ deposited on $[Cu_2(1,4\text{-ndc})_2(dabco)]_n$ in a layer-by-layer deposition approach on a self-assembled monolayer. Adapted from ref. 74 with permission from The Royal Society of Chemistry.

the $[Cu_2(1,4\text{-ndc})_2(dabco)]_n$ framework was again fabricated on a substrate of gold covered by a SAM of PPMT. To attain surface-selective functionalisation, a final $Cu(OAc)_2$ layer was deposited onto the already-formed MOF and followed by the introduction of an alternative ligand, 2-NH_2-1,4-bdc, which is added only on the surface of the MOF while the internal 1,4-ndc and dabco struts remain unchanged. This process effectively creates a lattice-matched monolayer of $[Cu_2(2\text{-}NH_2\text{-}1,4\text{-bdc})_2(dabco)]_n$ on the framework surface (Fig. 22).

Covalent PSM was utilised in this study to detect and confirm the presence of the newly-introduced amino groups and verify the functionalisation method's selectivity for the surface. Following the addition of the 2-NH_2-1,4-bdc mono-layer, the framework was exposed to fluorescein isothiocyanate (FITC) for subsequent analysis by fluorescence microscopy. FITC has been successfully used to image MOF surfaces in previously discussed examples, as it is too large to fit into the pores of some MOFs, confining it to reaction with primary amines only at the surface. Samples of both the unfunctiona-lised and amino-functionalised MOFs were exposed to FITC and examined by fluorescence microscopy; images of each framework without FITC treatment were also obtained as control samples. The lack of fluorescence from the untreated MOFs verifies that the fluorescence detected is as a result of the FITC tags covalently bonding to the amino groups present on the functionalised MOF surface, whereas fluorescence intensity was much weaker in the unfunctionalised FITC-treated MOF as there were no amino groups for FITC to react with. FITC uptake was also monitored by quartz crystal microbalance (QCM) analysis, which measures the differences in mass attached to the gold surface. QCM determined that the amino ligands were deposited on the surface and that FITC adhered only to the amino-functionalised framework, supporting the information obtained from fluorescence microscopy.
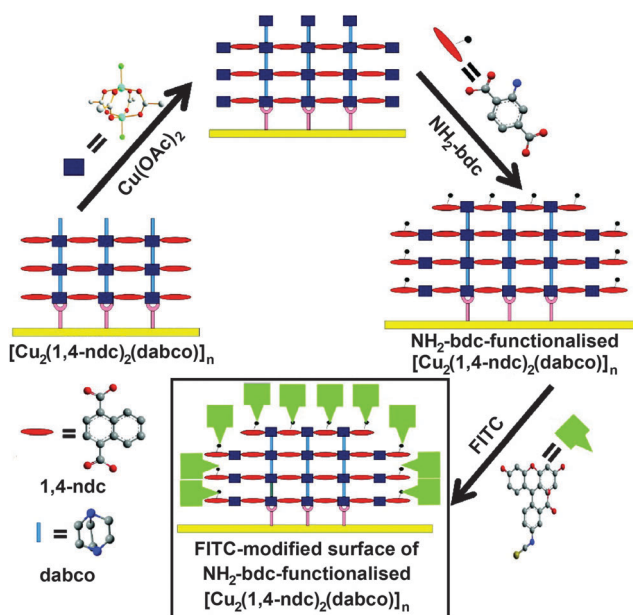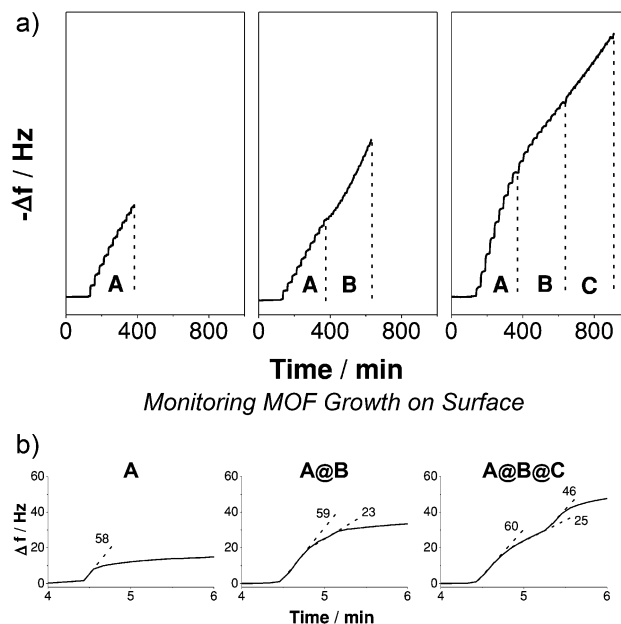
Fig. 22 Assembly of a thin film of $[Cu_2(1,4\text{-}ndc)_2(dabco)]_n$ on a gold surface, followed by addition of a monolayer of 2-NH$_2$-1,4-bdc on the outer surface of the film, using a layer–by–layer deposition approach. The outer layer can then be further functionalised by post-synthetic modification, in this case, tagging FITC units to the reactive amino functions. Reprinted (adapted) with permission from ref. 75. Copyright (2011) American Chemical Society.

Fig. 23 A quartz crystal microbalance (QCM) can be used to monitor (a) the stepwise deposition and growth of a ternary MOF thin film, A@B@C, on a surface, and (b) the distinct sorption profiles for films of varying compositions, with stepped sorption curves suggesting mono-, bi- or tri-layer MOF thin film structures. Reprinted (adapted) with permission from ref. 78. Copyright (2013) John Wiley and Sons.

The QCM technique is a powerful one, capable of measuring small mass changes from post-synthetic modification as well as uptake of guests in the resulting film, and it can also give insight into the kinetics of MOF crystallisation.[76] Fischer *et al.* demonstrated[77] this versatility in a similar example to those discussed previously, wherein a thin film of $[Cu_2(1,4\text{-}bdc)_2(dabco)]_n$ was prepared by LBL deposition and its surfaces covered, in a liquid phase heteroepitaxial surface growth experiment, by the amino-functionalised $[Cu_2(2\text{-}NH_2\text{-}1,4\text{-}bdc)_2(dabco)]_n$. QCM detected the subsequent post-synthetic surface modification by *t*-butyl isothiocyanate, which shows no fluorescence, and the hybrid film showed altered adsorption properties when compared to the unfunctionalised one, thought to be a consequence of the steric bulk introduced during surface modification limiting the pore apertures of the film.

Fischer *et al.* further expanded[78] the scope of the technique to encompass a trilayer system, wherein a base film of $[Cu_2(1,4\text{-}bdc)_2(dabco)]_n$ was surface modified with $[Cu_2(2\text{-}NH_2\text{-}1,4\text{-}bdc)_2(dabco)]_n$ and the hybrid film capped with $[Cu_2(1,4\text{-}ndc)_2(dabco)]_n$, with the LBL epitaxial growth monitored again by QCM (Fig. 23a) and X-ray diffraction analysis. The ternary structure was comprised of 15 cycles each of the three constituent frameworks, with the central 15 layers exhibiting NH$_2$ groups for covalent post-synthetic modification. Exposure to 4-fluorophenyl isothiocyanate resulted in covalent attachment to the NH$_2$ groups *via* thiourea formation, as monitored by infrared reflection absorption spectroscopy, while the separate chemi- and physisorption profiles of the volatile guest could be

distinguished by QCM (Fig. 23b). Indeed, a three-step absorption profile, consistent with the physi/chemi/physi-sorption properties of the three layers of the ternary hybrid, was observed, indicating the significant influence on materials properties that can be induced by hybrid MOF assembly.

The previous examples have all involved epitaxial growth of lattice-matched MOFs. The use of solely terephthalate based diacid linkers with dabco pillars means, in common with so-called multivariate MOFs,[79] all components of the hybrid MOFs have very similar unit cell parameters, and so layer by layer growth can proceed in a simple manner. A final example from the Fischer group has shown[80] that lattice-matching is not always necessary to produce bilayer thin films, with the successful heteroepitaxial growth of a layer of HKUST-1 – $[Cu_3(1,3,5\text{-}btc)_2]_n$ – atop a thin film of $[Cu_2(1,4\text{-}bdc)_2(dabco)]_n$. The $[Cu_2(1,4\text{-}bdc)_2(dabco)]_n$ thin film presents its [001] face, complete with N-donor dabco units, for further functionalisation, and in doing so acts in a similar manner to the pyridino self-assembled monolayer on which the MOF thin films are grown (Fig. 24). As such, HKUST-1 can subsequently be deposited on $[Cu_2(1,4\text{-}bdc)_2(dabco)]_n$ and crystal growth propagated in the [111] plane, as observed by out of plane X-ray diffraction and QCM analysis, consistent with previous investigations[81] into its growth on pyridino-based SAMs on gold. Absorption properties could also be measured, again using QCM analysis, with the hybrid film showing different properties towards sorption of methanol and mesitylene when compared to its individual constituents.
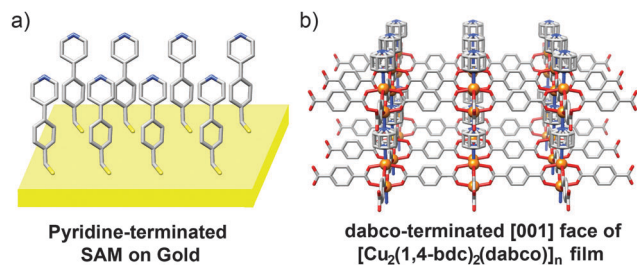
Fig. 24 Comparison of (a) an idealised self-assembled monolayer of PPMT on a gold surface and (b) the [001] face of [Cu₂(1,4-bdc)₂(dabco)]ₙ, both of which present N-donor ligands for deposition of a MOF thin film. Both substrates can be surface functionalised with a layer of HKUST-1.

Both layer-by-layer deposition and bulk core–shell MOF assembly demonstrate the potential for advanced materials with otherwise unattainable properties through utilizing epitaxial growth, with properties of hybrids far superior to simple mixtures of their constituent MOFs. The ability to combine several MOFs into an integrated multifunctional material could lead[69] to materials capable of both catalytic synthesis and purification, or simultaneous separation and trapping, with additional tailored properties, for example sensing, available through selective post-synthetic modification. One limitation is the almost ubiquitous need for lattice-matching to ensure appropriate MOF-on-MOF growth, although the final example in this section shows that this may eventually be overcome.

5. Conclusions and outlook

In this *Feature Article*, we have discussed the variety of methods now available to the synthetic chemist for controlling the surface chemistry of metal–organic frameworks. Coordination modulation allows control over the size of MOF particles as well as their surface chemistry, although it is not always the case that surface functionality is installed during the MOF synthesis. A variety of surface-selective post-synthetic surface modification methods have been developed, usually relying on the steric bulk of a reagent or surface ligand not allowing its penetration of the MOF. Careful experimental design is necessary to ensure that the surface coverage does not block the pores, although surface modification can be used to seal cargo within the confines of the MOF if desired. The added functionality that can be incorporated through surface-only covalent, coordinative and supramolecular interactions, as well as through ligand or metal exchange, has been demonstrated to enhance stability as well as adsorption properties. Similarly, direct growth of MOFs onto the surfaces of others has allowed the assembly of hybrids with properties unavailable to the individual constituents alone, and this can be carried out in bulk materials or in exquisitely constructed MOF thin films.

These breakthroughs have shown that controlling the surface chemistry of MOFs can have a dramatic effect on their properties and thus their suitability for application in a number of areas. Selective, targeted drug delivery can certainly benefit

from these advances, particularly considering the recent developments in conjugating complex biomolecules to MOFs. Surface modification can enhance the selectivity and storage capacities of MOFs in the adsorption and separation of small molecules, and also improve the catalytic selectivity of MOFs through restricted access of certain substrates to active sites. The ability to control the molecules bound to the surface of a MOF will undoubtedly revolutionise their processability and incorporation into hybrid materials, for example, in blending with polymers and assembly into membranes, as well as the preparation of composite materials containing multiple integrated MOF units with different functionalities.

The wide range of properties of MOFs – different pore sizes, metal ion(s), ligand(s), stabilities, *etc.* – means that the synthetic protocols discussed in this *Feature Article* are often developed with specific systems in mind. More general surface modification methods with a wide range of substrate tolerance would obviously be desirable, and could conceivably result from combinations of those currently available. The mild reactions which fall under the umbrella of click chemistry will continue to be essential to ensure more delicate MOF materials survive the surface functionalisation process with their porous structures intact, although robust materials, such as the examples based on Zr^{4+} cations, will also be ubiquitous. With the development of further experimental techniques, it may soon be a simpler task to tune the properties of MOFs by functionalisation of their surfaces rather than the entire bulk material.

Abbreviations

acac	Acetylacetonate
ad	Adeninate
adc	Anthracenedicarboxylate
AFM	Atomic force microscopy
bdc	Benzenedicarboxylate
BODIPY	Boron dipyrromethene
bpe	Bis(4-pyridyl)ethylene
bim	Benzimidazolate
bipy	Bipyridine
bpydc	2,2′-Bipyridine-5,5′-dicarboxylate
btc	Benzenetricarboxylate
CLSM	Confocal laser scanning microscopy
CuAAC	Copper-catalysed azide–alkyne cycloaddition
dabco	1,4-Diazabicyclo[2.2.2]octane
DBCO	Dibenzocyclooctyne
DCC	Dicyclohexylcarbodiimide
DMBIM	5,6-Dimethylbenzimidazole
DMF	*N,N*′-Dimethylformamide
DNA	Deoxyribonucleic acid
DPA	Dipicolinic acid
dpndi	*N,N*′-Di(4-pyridyl)-1,4,5,8-naphthalenetetracarboxydiimide
EBM	Ethidium bromide monoazide
EDC	1-Ethyl-3-(3-dimethylaminopropyl)carbodiimide
EGFP	Enhanced green fluorescent protein

FITC	Fluorescein isothiocyanate
FMA	Fluorescein-*O*-methacrylate
ICPOES	Inductively coupled plasma optical emission spectroscopy
IRMOF	Isoreticular metal–organic framework
LBL	Layer-by-layer
MALDI-TOF	Matrix-assisted laser desorption ionisation time-of-flight
MIL	Material of the institut Lavoisier
mim	2-Methylimidazolate
MOF	Metal–organic framework
M_W	Molecular weight
NAOS	*N*-Acryloxysuccinimide
ndc	Naphthalenedicarboxylate
NHS	*N*-Hydroxysuccinimide
NIPAM	*N*-Isopropylacrylamide
NMR	Nuclear magnetic resonance
pda	Phenylenediacetate
PCP	Porous coordination polymer
PEG	Poly(ethylene glycol)
pfmbc	*para*-Perfluoromethylbenzenecarboxylate
PPMT	4,4′-Pyridylphenylmethanethiol
PSM	Post-synthetic modification
PVP	Poly(vinylpyrrolidone)
QCM	Quartz crystal microbalance
SAM	Self-assembled monolayer
SBU	Secondary building unit
SEM	Scanning electron microscopy
TBDMS	*tert*-Butyldimethylsilyl
tcpb	Tetrakis(4-carboxyphenyl)benzene
TBA	Tetra-*n*-butylammonium
TEOS	Tetraethylorthosilicate
TFA	Trifluoroacetic acid
TGA	Thermogravimetric analysis
THF	Tetrahydrofuran
TMS	Trimethylsilyl
ZIF	Zeolitic imidazolate framework

Acknowledgements

Notes and references

1 (a) S. Kitagawa, R. Kitaura and S.-I. Noro, *Angew. Chem., Int. Ed.*, 2004, **43**, 2334–2375; (b) S. Kitagawa and R. Matsuda, *Coord. Chem. Rev.*, 2007, **251**, 2490–2509; (c) G. Férey, *Chem. Soc. Rev.*, 2008, **37**, 191–214; (d) J. R. Long and O. M. Yaghi, *Chem. Soc. Rev.*, 2009, **38**, 1213–1214, and other articles in this themed issue; (e) H.-C. Zhou, J. R. Long and O. M. Yaghi, *Chem. Rev.*, 2012, **112**, 673–674 and other articles in this themed issue; (f) H.-C. Zhou and S. Kitagawa, *Chem. Soc. Rev.*, 2014, **43**, 5415–5418 and other articles in this themed issue.
2 (a) J.-R. Li, Y. Ma, M. C. McCarthy, J. Sculley, J. Yu, H.-K. Jeong, P. B. Balbuena and H.-C. Zhou, *Coord. Chem. Rev.*, 2011, **255**, 1791–1823; (b) K. Sumida, D. L. Rogow, J. A. Mason, T. M. McDonald, E. D. Bloch, Z. R. Herm, T.-H. Bae and J. R. Long, *Chem. Rev.*, 2012, **112**, 724–781.
3 (a) L. J. Murray, M. Dincă and J. R. Long, *Chem. Soc. Rev.*, 2009, **38**, 1294–1314; (b) M. P. Suh, H. J. Park, T. K. Prasad and D.-W. Lim, *Chem. Rev.*, 2012, **112**, 782–835.
4 (a) R. E. Morris and P. S. Wheatley, *Angew. Chem., Int. Ed.*, 2008, **47**, 4966–4981; (b) J. R. Li, R. J. Kuppler and H. C. Zhou, *Chem. Soc. Rev.*, 2009, **38**, 1477–1504.
5 (a) J.-R. Li, J. Sculley and H.-C. Zhou, *Chem. Rev.*, 2012, **112**, 869–932; (b) B. Van de Voorde, B. Bueken, J. Denayer and D. De Vos, *Chem. Soc. Rev.*, 2014, **43**, 5766–5788.
6 (a) I. Imaz, M. Rubio-Martinez, J. An, I. Sole-Font, N. L. Rosi and D. Maspoch, *Chem. Commun.*, 2011, **47**, 7287–7302; (b) P. Horcajada, R. Gref, T. Baati, P. K. Allan, G. Maurin, P. Couvreur, G. Férey, R. E. Morris and C. Serre, *Chem. Rev.*, 2012, **112**, 1232–1268.
7 (a) J. Lee, O. K. Farha, J. Roberts, K. A. Scheidt, S. T. Nguyen and J. T. Hupp, *Chem. Soc. Rev.*, 2009, **38**, 1450–1459; (b) D. Farrusseng, S. Aguado and C. Pinel, *Angew. Chem., Int. Ed.*, 2009, **48**, 7502–7513; (c) L. Q. Ma, C. Abney and W. B. Lin, *Chem. Soc. Rev.*, 2009, **38**, 1248–1256; (d) A. Corma, H. García and F. X. Llabrés i Xamena, *Chem. Rev.*, 2010, **110**, 4606–4655; (e) J. Gascon, A. Corma, F. Kapteijn and F. X. Llabrés i Xamena, *ACS Catal.*, 2014, **4**, 361–378; (f) J. Liu, L. Chen, H. Cui, J. Zhang, L. Zhang and C.-Y. Su, *Chem. Soc. Rev.*, 2014, **43**, 6011–6061.
8 V. Stavila, A. A. Talin and M. D. Allendorf, *Chem. Soc. Rev.*, 2014, **43**, 5994–6010.
9 (a) R. A. Smaldone, R. S. Forgan, H. Furukawa, J. J. Gassensmith, A. M. Z. Slawin, O. M. Yaghi and J. F. Stoddart, *Angew. Chem., Int. Ed.*, 2010, **49**, 8630–8634; (b) J. J. Gassensmith, H. Furukawa, R. A. Smaldone, R. S. Forgan, Y. Y. Botros, O. M. Yaghi and J. F. Stoddart, *J. Am. Chem. Soc.*, 2011, **133**, 15312–15315.
10 (a) J. M. Roberts, B. M. Fini, A. A. Sarjeant, O. K. Farha, J. T. Hupp and K. A. Scheidt, *J. Am. Chem. Soc.*, 2012, **134**, 3334–3337; (b) P. W. Siu, Z. J. Brown, O. K. Farha, J. T. Hupp and K. A. Scheidt, *Chem. Commun.*, 2013, **49**, 10920–10922.
11 (a) E. D. Bloch, W. L. Queen, R. Krishna, J. M. Zadrozny, C. M. Brown and J. R. Long, *Science*, 2012, **335**, 1606–1610; (b) S. J. Geier, J. A. Mason, E. D. Bloch, W. L. Queen, M. R. Hudson, C. M. Brown and J. R. Long, *Chem. Sci.*, 2013, **4**, 2054–2061.
12 D. Zacher, R. Schmid, C. Wöll and R. A. Fischer, *Angew. Chem., Int. Ed.*, 2011, **50**, 176–199.
13 M. W. Ambrogio, C. R. Thomas, Y.-L. Zhao, J. I. Zink and J. F. Stoddart, *Acc. Chem. Res.*, 2011, **44**, 903–913.
14 D. A. Giljohann, D. S. Seferos, W. L. Daniel, M. D. Massich, P. C. Patel and C. A. Mirkin, *Angew. Chem., Int. Ed.*, 2010, **49**, 3280–3294.
15 S. Hermes, T. Witte, T. Hikov, D. Zacher, S. Bahnmüller, G. Langstein, K. Huber and R. A. Fischer, *J. Am. Chem. Soc.*, 2007, **129**, 5324–5325.
16 S. Diring, S. Furukawa, Y. Takashima, T. Tsuruoka and S. Kitagawa, *Chem. Mater.*, 2010, **22**, 4531–4538.
17 A. Umemura, S. Diring, S. Furukawa, H. Uehara, T. Tsuruoka and S. Kitagawa, *J. Am. Chem. Soc.*, 2011, **133**, 15506–15513.
18 F. Wang, H. Guo, Y. Chai, Y. Li and C. Liu, *Microporous Mesoporous Mater.*, 2013, **173**, 181–188.
19 (a) H. Guo, Y. Zhu, S. Qiu, J. A. Lercher and H. Zhang, *Adv. Mater.*, 2010, **22**, 4190–4192; (b) H. Guo, Y. Zhu, S. Wang, S. Su, L. Zhou and H. Zhang, *Chem. Mater.*, 2012, **24**, 444–450.
20 M. Goesten, E. Stavitski, E. A. Pidko, C. Gücüyener, B. Boshuizen, S. N. Ehrlich, E. J. M. Hensen, F. Kapteijn and J. Gascon, *Chem. – Eur. J.*, 2013, **19**, 7809–7816.
21 L.-N. Jin, Q. Liu and W.-Y. Sun, *CrystEngComm*, 2013, **15**, 4779–4784.
22 D. Jiang, A. D. Burrows and K. J. Edler, *CrystEngComm*, 2011, **13**, 6916–6919.
23 J. M. Chin, E. Y. Chen, A. G. Menon, H. Y. Tan, A. T. S. Hor, M. K. Schreyer and J. Xu, *CrystEngComm*, 2013, **15**, 654–657.
24 A. Schaate, P. Roy, A. Godt, J. Lippke, F. Waltz, M. Wiebcke and P. Behrens, *Chem. – Eur. J.*, 2011, **17**, 6643–6651.
25 J. Cravillon, R. Nayuk, S. Springer, A. Feldhoff, K. Huber and M. Wiebcke, *Chem. Mater.*, 2011, **23**, 2130–2141.
26 J. Cravillon, C. A. Schroder, H. Bux, A. Rothkirch, J. Caro and M. Wiebcke, *CrystEngComm*, 2012, **14**, 492–498.
27 J. Park, Z. U. Wang, L.-B. Sun, Y.-P. Chen and H.-C. Zhou, *J. Am. Chem. Soc.*, 2012, **134**, 20110–20116.
28 F. Vermoortele, B. Bueken, G. Le Bars, B. Van de Voorde, M. Vandichel, K. Houthoofd, A. Vimont, M. Daturi, M. Waroquier, V. Van Speybroeck, C. Kirschhock and D. E. De Vos, *J. Am. Chem. Soc.*, 2013, **135**, 11465–11468.

29 J. Zhao, Y. Guo, H. Guo, Y. Chai, Y. Li, Y. Liu and C. Liu, *Inorg. Chem. Commun.*, 2012, **18**, 21–24.

30 T. Tsuruoka, S. Furukawa, Y. Takashima, K. Yoshida, S. Isoda and S. Kitagawa, *Angew. Chem., Int. Ed.*, 2009, **48**, 4739–4743.

31 Y. Sakata, S. Furukawa, C. Kim and S. Kitagawa, *Chem. Lett.*, 2012, **41**, 1436–1438.

32 M.-H. Pham, G.-T. Vuong, F.-G. Fontaine and T.-O. Do, *Cryst. Growth Des.*, 2012, **12**, 3091–3095.

33 Y. Sakata, S. Furukawa, M. Kondo, K. Hirai, N. Horike, Y. Takashima, H. Uehara, N. Louvain, M. Meilikhov, T. Tsuruoka, S. Isoda, W. Kosaka, O. Sakata and S. Kitagawa, *Science*, 2013, **339**, 193–196.

34 N. Yanai and S. Granick, *Angew. Chem., Int. Ed.*, 2012, **51**, 5638–5641.

35 N. Yanai, M. Sindoro, J. Yan and S. Granick, *J. Am. Chem. Soc.*, 2013, **135**, 34–37.

36 (*a*) Z. Wang and S. M. Cohen, *Chem. Soc. Rev.*, 2009, **38**, 1315–1329; (*b*) A. D. Burrows, *CrystEngComm*, 2011, **13**, 3623–3642; (*c*) S. M. Cohen, *Chem. Rev.*, 2012, **112**, 970–1000.

37 J. Della Rocca, D. Liu and W. Lin, *Acc. Chem. Res.*, 2011, **44**, 957–968.

38 W. J. Rieter, K. M. L. Taylor and W. Lin, *J. Am. Chem. Soc.*, 2007, **129**, 9852–9853.

39 K. M. L. Taylor, W. J. Rieter and W. Lin, *J. Am. Chem. Soc.*, 2008, **130**, 14358–14359.

40 W. J. Rieter, K. M. Pott, K. M. L. Taylor and W. Lin, *J. Am. Chem. Soc.*, 2008, **130**, 11584–11585.

41 Z. Li and H. C. Zeng, *J. Am. Chem. Soc.*, 2014, **136**, 5631–5639.

42 D. Liu, R. C. Huxford and W. Lin, *Angew. Chem., Int. Ed.*, 2011, **50**, 3696–3700.

43 K. M. L. Taylor-Pashow, J. Della Rocca, Z. G. Xie, S. Tran and W. B. Lin, *J. Am. Chem. Soc.*, 2009, **131**, 14261–14263.

44 P. Horcajada, T. Chalati, C. Serre, B. Gillet, C. Sebrie, T. Baati, J. F. Eubank, D. Heurtaux, P. Clayette, C. Kreuz, J.-S. Chang, Y. K. Hwang, V. Marsaud, P.-N. Bories, L. Cynober, S. Gil, G. Férey, P. Couvreur and R. Gref, *Nat. Mater.*, 2010, **9**, 172–178.

45 M. D. Rowe, H. T. Thamm, S. L. Kraft and S. G. Boyes, *Biomacromolecules*, 2009, **10**, 983–993.

46 R. C. Huxford, K. E. deKrafft, W. S. Boyle, D. Liu and W. Lin, *Chem. Sci.*, 2012, **3**, 198–204.

47 J. Chun, S. Kang, N. Park, E. J. Park, X. Jin, K.-D. Kim, H. O. Seo, S. M. Lee, H. J. Kim, W. H. Kwon, Y.-K. Park, J. M. Kim, Y. D. Kim and S. U. Son, *J. Am. Chem. Soc.*, 2014, **136**, 6786–6789.

48 (*a*) O. Karagiaridi, W. Bury, J. E. Mondloch, J. T. Hupp and O. K. Farha, *Angew. Chem., Int. Ed.*, 2014, **53**, 4530–4540; (*b*) Y. Han, J.-R. Li, Y. Xie and G. Guo, *Chem. Soc. Rev.*, 2014, **43**, 5952–5981.

49 M. Kondo, S. Furukawa, K. Hirai and S. Kitagawa, *Angew. Chem., Int. Ed.*, 2010, **49**, 5327–5330.

50 X. Liu, Y. Li, Y. Ban, Y. Peng, H. Jin, H. Bux, L. Xu, J. Caro and W. Yang, *Chem. Commun.*, 2013, **49**, 9140–9142.

51 X. Song, T. K. Kim, H. Kim, D. Kim, S. Jeong, H. R. Moon and M. S. Lah, *Chem. Mater.*, 2012, **24**, 3065–3073.

52 A. M. Shultz, O. K. Farha, D. Adhikari, A. A. Sarjeant, J. T. Hupp and S. T. Nguyen, *Inorg. Chem.*, 2011, **50**, 3174–3176.

53 H. G. T. Nguyen, M. H. Weston, O. K. Farha, J. T. Hupp and S. T. Nguyen, *CrystEngComm*, 2012, **14**, 4115–4118.

54 K. Hirai, K. Chen, T. Fukushima, S. Horike, M. Kondo, N. Louvain, C. Kim, Y. Sakata, M. Meilikhov, O. Sakata, S. Kitagawa and S. Furukawa, *Dalton Trans.*, 2013, **42**, 15868–15872.

55 K. K. Tanabe, Z. Wang and S. M. Cohen, *J. Am. Chem. Soc.*, 2008, **130**, 8508–8517.

56 M. Ma, A. Gross, D. Zacher, A. Pinto, H. Noei, Y. Wang, R. A. Fischer and N. Metzler-Nolte, *CrystEngComm*, 2011, **13**, 2828–2832.

57 S. Jung, Y. Kim, S.-J. Kim, T.-H. Kwon, S. Huh and S. Park, *Chem. Commun.*, 2011, **47**, 2904–2906.

58 Y. Goto, H. Sato, S. Shinkai and K. Sada, *J. Am. Chem. Soc.*, 2008, **130**, 14354–14355.

59 W. Morris, W. E. Briley, E. Auyeung, M. D. Cabezas and C. A. Mirkin, *J. Am. Chem. Soc.*, 2014, **136**, 7261–7264.

60 T. Gadzikwa, G. Lu, C. L. Stern, S. R. Wilson, J. T. Hupp and S. T. Nguyen, *Chem. Commun.*, 2008, 5493–5495.

61 T. Gadzikwa, O. K. Farha, C. D. Malliakas, M. G. Kanatzidis, J. T. Hupp and S. T. Nguyen, *J. Am. Chem. Soc.*, 2009, **131**, 13613–13615.

62 S. Nagata, H. Sato, K. Sugikawa, K. Kokado and K. Sada, *CrystEngComm*, 2012, **14**, 4137–4141.

63 P. Roy, A. Schaate, P. Behrens and A. Godt, *Chem. – Eur. J.*, 2012, **18**, 6979–6985.

64 S. Furukawa, K. Hirai, K. Nakagawa, Y. Takashima, R. Matsuda, T. Tsuruoka, M. Kondo, R. Haruki, D. Tanaka, H. Sakamoto, S. Shimomura, O. Sakata and S. Kitagawa, *Angew. Chem.*, 2009, **121**, 1798–1802.

65 K. Koh, A. G. Wong-Foy and A. J. Matzger, *Chem. Commun.*, 2009, 6162–6164.

66 Y. Yoo and H.-K. Jeong, *Cryst. Growth Des.*, 2010, **10**, 1283–1288.

67 P. A. Szilágyi, M. Lutz, J. Gascon, J. Juan-Alcañiz, J. van Esch, F. Kapteijn, H. Geerlings, B. Dam and R. van de Krol, *CrystEngComm*, 2013, **15**, 6003–6008.

68 S. Furukawa, K. Hirai, Y. Takashima, K. Nakagawa, M. Kondo, T. Tsuruoka, O. Sakata and S. Kitagawa, *Chem. Commun.*, 2009, 5097–5099.

69 K. Hirai, S. Furukawa, M. Kondo, H. Uehara, O. Sakata and S. Kitagawa, *Angew. Chem., Int. Ed.*, 2011, **50**, 8057–8061.

70 K. Hirai, S. Furukawa, M. Kondo, M. Meilikhov, Y. Sakata, O. Sakata and S. Kitagawa, *Chem. Commun.*, 2012, **48**, 6472–6474.

71 T. Li, J. E. Sullivan and N. L. Rosi, *J. Am. Chem. Soc.*, 2013, **135**, 9984–9987.

72 (*a*) D. Zacher, O. Shekhah, C. Woll and R. A. Fischer, *Chem. Soc. Rev.*, 2009, **38**, 1418–1429; (*b*) D. Bradshaw, A. Garai and J. Huo, *Chem. Soc. Rev.*, 2012, **41**, 2344–2381; (*c*) A. Bétard and R. A. Fischer, *Chem. Rev.*, 2012, **112**, 1055–1083.

73 O. Shekhah, H. Wang, S. Kowarik, F. Schreiber, M. Paulus, M. Tolan, C. Sternemann, F. Evers, D. Zacher, R. A. Fischer and C. Wöll, *J. Am. Chem. Soc.*, 2007, **129**, 15118–15119.

74 O. Shekhah, K. Hirai, H. Wang, H. Uehara, M. Kondo, S. Diring, D. Zacher, R. A. Fischer, O. Sakata, S. Kitagawa, S. Furukawa and C. Woll, *Dalton Trans.*, 2011, **40**, 4954–4958.

75 B. Liu, M. Ma, D. Zacher, A. Bétard, K. Yusenko, N. Metzler-Nolte, C. Wöll and R. A. Fischer, *J. Am. Chem. Soc.*, 2011, **133**, 1734–1737.

76 V. Stavila, J. Volponi, A. M. Katzenmeyer, M. C. Dixon and M. D. Allendorf, *Chem. Sci.*, 2012, **3**, 1531–1540.

77 M. Tu, S. Wannapaiboon and R. A. Fischer, *Dalton Trans.*, 2013, **42**, 16029–16035.

78 B. Liu, M. Tu, D. Zacher and R. A. Fischer, *Adv. Funct. Mater.*, 2013, **23**, 3790–3798.

79 H. Deng, C. J. Doonan, H. Furukawa, R. B. Ferreira, J. Towne, C. B. Knobler, B. Wang and O. M. Yaghi, *Science*, 2010, **327**, 846–850.

80 M. Tu and R. A. Fischer, *J. Mater. Chem. A*, 2014, **2**, 2018–2022.

81 O. Shekhah, H. Wang, D. Zacher, R. A. Fischer and C. Wöll, *Angew. Chem., Int. Ed.*, 2009, **48**, 5038–5041.